

Interpretable Melanoma Detection for a Clinical Environment

Elliot Naylor



Submitted in accordance with the requirements for the degree of
Doctor of Philosophy

University of South Wales
Faculty of Mathematics and Computing

Date

The candidate confirms that the work submitted is his/her own and that appropriate credit has been given where reference has been made to the work of others.

This copy has been supplied on the understanding that it is copyright material and that no quotation from the thesis may be published without proper acknowledgement.

The right of Elliot Naylor to be identified as Author of this work has been asserted by him/her in accordance with the Copyright, Designs and Patents Act 1988.

©Year
University of South Wales
and
Candidate Elliot Naylor

Dedication here.

Acknowledgements

Abstract

Contents

| | | |
|----------|--|----------|
| 1 | Introduction | 2 |
| 1.1 | Background | 2 |
| 1.1.1 | Diagnostic Procedures (ABCD Rules, CASH, 7-Point Checklist, Texture) | 3 |
| 1.1.2 | UI Development and visualisation | 3 |
| 1.1.3 | Conclusion | 5 |
| 1.2 | Purpose and Research Questions | 6 |
| 1.3 | Scope and Limitations (Use-Case) | 6 |
| 1.4 | Target Group | 6 |
| 1.5 | Aim | 7 |
| 1.6 | Objectives | 7 |
| 1.7 | Contributions to knowledge | 7 |
| 2 | Systematic Review | 9 |
| 2.1 | Introduction | 9 |
| 2.2 | Skin Lesions | 9 |
| 2.3 | Diagnostic Procedures | 9 |
| 2.4 | CAD Systems for Skin Lesion Diagnosis | 9 |
| 2.5 | Case-Based Reasoning | 9 |
| 2.6 | Discussion | 9 |
| 2.7 | Research Methodology | 10 |
| 2.7.1 | Research Questions | 10 |
| 2.7.2 | Search Criteria | 10 |
| 2.8 | Artificial Neural Network (ANN) Techniques | 10 |
| 2.9 | Convolutional Neural Network (CNN) Techniques | 11 |
| 2.10 | Deep Neural Network (DNN) Techniques | 11 |
| 2.11 | Kohonen Self-Organising Neural Network (KNN) Techniques | 11 |
| 2.12 | Generative Adversarial Network (GAN) Techniques | 11 |
| 2.13 | Explainability Techniques | 11 |
| 2.14 | Ensemble Learning Techniques | 11 |

| | | |
|----------|---|-----------|
| 2.15 | Hybrid machine learning techniques | 11 |
| 2.16 | Feature Extraction Techniques | 12 |
| 2.16.1 | Segmentation | 12 |
| 2.16.2 | Handcrafted Features | 13 |
| 2.16.3 | Combining ABCD Rules | 16 |
| 2.17 | Datasets | 17 |
| 2.18 | Challenges of Explainability | 17 |
| 2.19 | Conclusion and Future Work | 17 |
| 3 | Dataset Suitability for Melanoma Detection | 18 |
| 3.1 | Introduction | 18 |
| 3.2 | Other Datasets | 18 |
| 3.3 | Issues | 19 |
| 3.3.1 | ISIC | 20 |
| 3.3.2 | PH2 | 28 |
| 3.3.3 | Diagnosis and Image Assessment | 34 |
| 3.4 | Conclusion | 34 |
| 3.5 | Developing the NHS dataset | 35 |
| 3.5.1 | Requirements | 35 |
| 3.5.2 | Data Biases | 36 |
| 3.6 | Data Transformation and Analysis | 39 |
| 3.6.1 | Historical Diagnosis of Skin lesions | 39 |
| 3.6.2 | Anatomical location | 42 |
| 3.7 | Data Transformation and Augmentation | 43 |
| 3.7.1 | Hair Removal | 43 |
| 3.7.2 | Specular Removal | 43 |
| 3.8 | Conclusion | 44 |
| 3.9 | Dataset Statistics | 44 |
| 4 | Analysis of Explainability for the Detection of Melanoma | 49 |
| 4.1 | Introduction | 49 |
| 4.2 | Background | 49 |
| 4.2.1 | Dataset | 50 |
| 4.3 | DeepSHAP | 50 |
| 4.3.1 | Summary | 51 |
| 4.4 | Grad-Cam | 51 |
| 4.4.1 | Summary | 51 |
| 4.4.2 | Tree ensemble methods | 51 |
| 4.5 | Bayesian Network Approach | 51 |
| 4.6 | Conclusion | 51 |

| | | |
|----------|---|-----------|
| 5 | Implementation of segmentation, ABCD rules and Dermoscopic structures | 52 |
| 5.1 | Introduction | 52 |
| 5.2 | Hybrid Melanoma Segmentation Algorithms using Neural Networks and Statistical Models | 52 |
| 5.2.1 | Related Works | 53 |
| 5.2.2 | Semantic Pixel Wise Segmentation (SegNet) | 54 |
| 5.2.3 | U-Otsu Threshold | 54 |
| 5.2.4 | LBPC segmentation | 55 |
| 5.2.5 | Results | 56 |
| 5.2.6 | Results of Border Cut-off | 58 |
| 5.3 | Issues | 58 |
| 5.3.1 | Joint Neural network and statistical model approach | 58 |
| 5.4 | ABCD Rules Data Extraction Techniques | 58 |
| 5.4.1 | Preferred Diagnostic Procedures | 59 |
| 5.4.2 | Related Works | 60 |
| 5.5 | A Novel Asymmetry detection technique using Bi-Fold, 3D Euclidean distance, and Superpixels | 60 |
| 5.5.1 | Bi-fold | 61 |
| 5.5.2 | 3D Euclidean Distance | 61 |
| 5.5.3 | Superpixels using Simple Linear Iterative Clustering (SLIC) | 61 |
| 5.6 | Experimental Results | 62 |
| 5.7 | Border Detection Using Zernike Moments, Fractal Box-Counting, and Convexity | 65 |
| 5.8 | A Novel Colour Analysis Approach using Colour Ranges, and SVM | 65 |
| 5.9 | Dermoscopic structures | 65 |
| 5.10 | Results | 65 |
| 5.11 | Conclusion | 65 |
| 6 | Case-Based Reasoning (CBR) | 66 |
| 7 | Combined ABCD Rules and Dermoscopic Structures using Bayesian Network | 67 |
| 7.1 | Introduction | 67 |
| 7.2 | Background | 67 |
| 7.3 | Related Work | 68 |
| 7.3.1 | Feature Extraction algorithms | 68 |
| 7.3.2 | Classification Methods | 69 |
| 7.4 | Proposed Method | 69 |
| 7.4.1 | Feature Extraction Methods | 70 |
| 7.4.2 | Bayesian Fusion using Naive Bayes | 71 |
| 7.4.3 | Case-Based reasoning using Artificial Neural Network (ANN) | 71 |

| | | |
|-----------|----------------------|-----------|
| 7.5 | Results | 71 |
| 7.6 | Discussion | 71 |
| 7.7 | Conclusion | 71 |
| 8 | Conclusion | 72 |
| 9 | Future Work | 74 |
| 10 | Tables | 80 |
| 11 | Appendix | 81 |

List of Figures

| | | |
|------|--|----|
| 2.1 | Images of two skin lesions from the PH ² dataset showing the asymmetry calculated from moments. | 14 |
| 2.2 | Images of two skin lesions split into 8 sections using moments, each border is measured for irregularity. | 15 |
| 3.1 | Examples from the ISIC 2019 dataset, where first two images are BN, followed by two SK, and four MM. | 20 |
| 3.2 | ISIC 2019 dataset showing the number of image samples and the diagnosis of those skin lesions dataset appears to be highly unbalanced with half being NV. | 21 |
| 3.3 | The dataset has more male than female patients except for NV which has more samples. | 22 |
| 3.4 | This shows the number of image samples compared to the age, the dataset is largely unbalanced regarding age where patients are between 40 and 75 years of age. | 23 |
| 3.5 | The approximate age range of patients and their diagnosis. | 24 |
| 3.6 | Shows image examples associated with the anatomical location and age of the patients. | 25 |
| 3.7 | Shows image examples associated with the anatomical location and age of the patients. | 26 |
| 3.8 | Number of images containing dermoscopic structures. | 27 |
| 3.9 | Number of dermoscopic structures relating | 28 |
| 3.10 | Example of images from the PH2 dataset. The first two are standard, the second two are atypical, and the last 4 are melanoma. | 29 |
| 3.11 | Number of image samples and diagnosis in the PH2 dataset. | 30 |
| 3.12 | This shows the number of image samples and asymmetry score based on Total dermoscopy score (TDS). | 31 |
| 3.13 | Number of colours in the PH2 dataset compared with the diagnosis. Colours are in order white, red, light brown, dark brown, blue-gray, and black. | 31 |
| 3.14 | Dermoscopic structures and the number of images. These are labelled between absent, atypical, present, and Typical. | 32 |

| | | |
|------|--|----|
| 3.15 | Shows the labels of dermoscopic structures, number of images, and diagnosis. These are labelled between absent, atypical, present, and Typical. | 32 |
| 3.16 | Shows the number of images based on the diagnosis and dermoscopic structures present, typical, and atypical. | 33 |
| 3.17 | Pigment network data relating to the diagnosis. | 33 |
| 3.18 | Number of image samples relating to the historical diagnosis. Labelled as uncertain if there is a ‘?’ in the diagnosis. | 40 |
| 3.19 | Number of skin lesion samples with multiple diagnoses in the historical diagnoses. Other types including lentigo, Bowen’s disease, dermatofibroma, pyogenic granuloma, and wart are only associated with the main diagnoses (AN, BN, MM, SCC, BCC) because they are not specifically searched for. This means they are only found in association with the mentioned main diagnoses and this data is likely missing data comparing the other types. . . | 41 |
| 3.20 | Comparing skin lesions that are diagnosed as MM, SK, and considered both MM and SK. | 42 |
| 3.21 | Number of image samples relating to the diagnosis of the image. | 44 |
| 3.22 | Age of patients and number of image samples. | 45 |
| 3.23 | Number of image samples related to the location of the skin lesion. | 46 |
| 3.24 | Number of image samples relating to the diagnosis and sex of the patients. There are more female than male patients. | 47 |
| 3.25 | Boxplot describing the age of patients and the diagnosis. | 48 |
| 3.26 | Number of image samples relating to the diagnosis of the image. | 48 |
| 5.1 | Some images from the ISIC dataset demonstrating the difference between segmentation masks and expert segmentation masks. | 53 |
| 5.2 | Demonstrating the Semantic Pixel-Wise Segmentation (SegNet) results showing the a) original image, b) expert ground-truth and c) SegNet results. . . | 54 |
| 5.3 | Otsu thresholding alongside ground-truth mask, where grey Otsu and white is SegNet. The bar chart shows the histogram with an otsu threshold of 138. . . | 55 |
| 5.4 | Local Binary Pattern Clustering (LBPC) showing the a) original image, b) ground-truth, and c) LBPC. LBPC successfully exaggerates the border cut-off on the skin lesions with regular and irregular borders | 57 |
| 5.5 | This diagram is a summary of the PH2 dataset after using bi-fold, a euclidean distance of colour. The value on the right would be a threshold. | 62 |
| 5.6 | This diagram shows the skin lesion split relating to superpixels instead of averaging squares. | 63 |
| 5.7 | This diagram shows the difference between averaging squares and using superpixels, with the threshold of 10 implying curves and 50 being squares. The horizontal colour difference is improved, making it more likely to be seen asymmetrical. The vertical comparison is roughly the same, except for removing a false positive of 40. | 64 |

| | | |
|-----|---|----|
| 7.1 | Proposed CAD framework describing the segmentation, feature extraction and classification process. | 70 |
|-----|---|----|

List of Tables

| | | |
|-----|---|----|
| 1.1 | Total dermoscopy score (TDS) is a scoring system used with ABCD rules to support clinicians when diagnosing melanoma[12]. Each rule is multiplied by weights and the sum of the combined values is the final score, all together: $[(\text{Asymmetry} \times 1.3) + (\text{Border} \times 0.1) + (\text{Colour} \times 0.5) + (\text{Dermoscopic structure} \times 0.5)]$ | 4 |
| 3.1 | | 19 |
| 3.2 | | 20 |
| 3.3 | This table shows the metadata in each image and a description of each label. Rows highlighted in red are removed to protect patient confidentiality. . . . | 39 |
| 3.4 | Examples of historical diagnosis and doctors and some unique variations of labelling. | 40 |
| 3.5 | All the different labelling for the anatomical location of the lesion. Each label in the NHS data has been assigned to a category similar to the ISIC dataset. | 42 |

Chapter 1

Introduction

1.1 Background

Skin cancer is considered amongst the most severe public health concerns, with mortality rates of 2,353 per 100,000 within the United Kingdom (UK) in 2018[44]. Skin cancers can be categorised between melanoma and non-melanoma, whereas melanoma is the most dangerous because it is unpredictable. When left untreated and after growing sufficiently, it can spread to other regions of the body (known as metastatic melanoma), which once progressed is challenging to treat effectively with a 10% survival over ten years in the US[10]. Furthermore, it is beneficial to catch melanoma early because it is the most easily treatable form of cancer, with 86% of cases being preventable[44]. However, melanoma can remain dormant from anywhere between 6 months to 10 years before maturing and becoming a danger to the patient[44]. Another danger of melanoma is its similarity to non-melanoma skin cancers, such as a mimic called seborrheic keratosis (SK), which frequently leads to misdiagnoses[18]. There are features unique to SK called fissures, ridges, and hairpin vessels[24]. Problematically these features require trained specialists to recognise them needing more than ten years of experience to have an accuracy of 86% compared to 62% or 56% (3 to 5 years of experience)[25]. However, because of the cost of training new doctors, there are limited available. Dermatologists primarily treat skin conditions (biopsies) and confirm diagnoses submitted by GP. General practitioners (GP) are the first to diagnose skin conditions and sometimes have limited experience diagnosing them (especially dermatological features). This project aims to improve the accuracy of GP observations by providing tools for the automatic classification of skin lesions. For the previously mentioned reasons, an automatic system should be cost-effective and advantageous to doctors.

1.1.1 Diagnostic Procedures (ABCD Rules, CASH, 7-Point Checklist, Texture)

Diagnostic procedures are instructions developed by doctors to simplify diagnosing conditions. Various methods have been developed to diagnose skin lesions and have greatly improved GP accuracy within clinical environments[27, 45]. Considering melanoma is the most dangerous skin condition, most procedures were developed specifically for early detection. Some include ABCD rules, 2-point checklist, 7-point checklist, and CASH. The most preferred of these techniques are ABCD rules and CASH because they have a higher sensitivity[45] and ABCD rules are generally the most preferred because it is easy to learn and is rapidly calculated[27]. There are several variations of ABCD rules, but, is originally measured using asymmetry, border, colour, and diameter. Diameter is sometimes replaced with dermatological structures because many features (i.e. blue-black signs, pigment networks, pseudopods, streaks, or milia-like cysts[37]) improve the classification accuracy between melanoma and the mimic seborrheic keratosis[12]. Furthermore, automatically measuring diameter is often difficult because it is dependent on the photo apparatus and the distance from the skin lesion, which is rarely consistent in research. Table 1.1.1 describes each rule in more detail, including a scoring system called total dermoscopy score (TDS), where each rule is assigned a score and combined to reach a result of either malignant, suspicious or benign. The criteria is: $[(\text{Asymmetry} \times 1.3) + (\text{Border} \times 0.1) + (\text{Colour} \times 0.5) + (\text{Dermoscopic structure} \times 0.5)]$. Each rule is calculated using the following descriptions in Table 1.1.1 and multiplied by their weight and then added together to reach a final score where $[< 4.76 = \text{benign}, > 4.76 \text{ or } < 5.45 = \text{suspicious}, > 5.45 = \text{melanoma}]$. The disadvantage is the subjectivity of GP observations relating to their experience. So, it would be beneficial to automate the techniques using algorithms to standardise results and improve GP accuracy.

1.1.2 UI Development and visualisation

The user interface (UI) being the method in which algorithms are visualised is arguably the most import section of this project because without the means of presenting algorithms in an explainable way they are of little to no use to healthcare professionals. Providing explanations will improve trust from doctors and patients to these algorithms[8]. This is also crucial for the successful implementation of AI technologies within healthcare settings[skar2017].

Computer-aided diagnostic (CAD) frameworks are a collection of algorithms designed to guide decision-making processes within clinical environments[14]. A paper written by Andre Estava demonstrates a deep convolutional neural network (DCNN) that has comparable accuracy to that of dermatologists, trained using 129,450 clinical images consisting of 2,032 different diseases[7]. DCNN generates a collection of artificial neurons organised into layers, where each neuron receives input from a previous layer to perform a computation. The

| Criteria | Methodology | Score | Weight |
|------------------------|---|-------|--------------|
| Asymmetry | Measuring asymmetry involves first finding the centroid and splitting it twice with a 90-degree axis. Each side is subtracted with its opposite half to measure the asymmetry of shape, colour, and dermoscopic structures. If both sides are asymmetrical then the score is 2, one side asymmetrical is a score of 1, and otherwise, the score is 0. | 0 - 2 | $\times 1.3$ |
| Border | border is found by finding the centroid and drawing lines through it with a 45-degree angle, splitting the skin lesion into eight segments. Border segments might be irregular with convexity, sharp corners, or edges. Irregular segments are incremented by 1, reaching 8 for each segment. | 0 - 8 | $\times 1.3$ |
| Colour | The area of the skin lesion is up to 6 colours (white, red, light brown, dark brown, blue-grey, black). The score is increased by 1 for each visible colour, reaching a total of 6. | 1 - 6 | $\times 0.5$ |
| Dermoscopic Structures | Dermoscopic structures are measured by finding structureless areas, pigment networks, atypical networks, dots, and globules. Each visible structure adds a score of 1, reaching a total of 5. | 1 - 5 | $\times 0.5$ |

Table 1.1: Total dermoscopy score (TDS) is a scoring system used with ABCD rules to support clinicians when diagnosing melanoma[12]. Each rule is multiplied by weights and the sum of the combined values is the final score, all together: $[(\text{Asymmetry} \times 1.3) + (\text{Border} \times 0.1) + (\text{Colour} \times 0.5) + (\text{Dermoscopic structure} \times 0.5)]$.

collection of layers is a network, which (once trained) ultimately measures the relationship between input parameters based on provided data. It is important to note that the accuracy is proportionate to the number of images and data quality for training that network. Unfortunately, these image samples are frequently private and unavailable to many institutions. Without adequate image data to test the capabilities of machine learning models, there is no method for measuring these biases and is therefore unsafe to use within clinical environments. Secondly, these approaches will often produce a parallel diagnosis, meaning that results are not always explainable[21]. There are many valuable techniques, but even the best techniques are inadequate for doctors without catering to interpretability. Other techniques are interpretable by considering diagnostic procedures, such as ABCD rules, many of which are described by Ali[5]. Techniques based on diagnostic procedures can be more easily tested for biases and provide further insight to GPs with the means to learn from and understand results. Techniques include support vector machine (SVM), a supervised machine learning that uses regression analysis to categorise labelled data into two or more groups. The advantage means less data for training is required, and the model is interpretable.

Doctors will often only have access to a patient for a short time before moving to another. CAD frameworks are beneficial because they speed up the process, can improve accuracy[14], and ensure the gathering of relevant data (ABCD rules). Furthermore, it could take days for a second opinion from another doctor, where an automatic system immediately provides it. Automated systems should also provide adequate explanations that can be understood quickly and easily by doctors[21]. One method is to provide visual explanations. Many authors[48, 19, 3] describe different ways to measure ABCD rules, including the asymmetry of skin lesions using bi-fold. Automated versions of the procedure use the centroid and moments of inertia to fold the skin lesion horizontally and vertically along the centroid. The overhung area on both axes is subtracted from the final score to measure asymmetrical or symmetrical. This technique produces an adequate visualisation that can provide GPs with an interpretable result. There is a range of other examples for ABCD rules, including border[19, 48, 4], colour[35, 41, 19], and dermoscopic structures[22] that use a range of interpretable algorithms that produce interpretable results.

1.1.3 Conclusion

Overall, many advanced machine learning techniques using neural networks lack the interpretability required within clinical environments. Furthermore, public datasets lack rarer skin conditions, making finding biases challenging. Automating the ABCD rules can solve this by using a technique that GPs are familiar with, and by using statistical models to extract relevant features (relating to the ABCD rules). This is followed by summarising rules using Bayesian fusion and calculating the significance of individual features.

1.2 Purpose and Research Questions

In this thesis machine learning algorithms were developed for the automatic classification of skin lesions with consideration for its use within clinical environments. Furthermore, the techniques need to produce an explainable and meaningful response that can support doctors (dermatologists and general practitioners) by providing insights and details that might have been missed. Concerning this, two main research questions:

- Are the produced algorithms accurate enough to be properly utilised in a clinical environment?
- Does the developed technique provide meaningful responses that can be properly utilised within a clinical environment?

1.3 Scope and Limitations (Use-Case)

Some limitations were set by the company partner based on where they plan to utilise the developed algorithms. In this case the technique is primarily going to be utilised by GP (general practitioners) that are unlikely to have the specific training and equipment for diagnosing skin lesions.

- The algorithms are developed for the detection of Benign Naevi (BN), Melanoma (MM), Seborrhoeic keratosis (SK), Atypical Naevi (AN), Typical Naevi (TN), Squamous Cell Carcinoma (SCC), Basal Cell Carcinoma (BCC). With a primary focus on SK considering its difficulty to diagnose.
- Macroscopic images will be analysed instead of dermoscopes. This essentially means a standard camera will be used, which includes variations in lighting which might obscure features in skin lesions.
- Meta-data includes area on body, gender, Date of Birth (DOB), department, Diagnosis. The goal is to utilise this data for automatic detection.
- Techniques must be explainable, so that doctors can recognise incorrect responses.

1.4 Target Group

The work is primarily for general practitioners (GPs) because it is usually the source of misdiagnosed skin lesions due to the lack of specific training compared to dermatologists. The goal is to improve the accuracy of techniques using a cheap device for capturing data, furthermore automatic classification should provide a more adequate means for dermatologists to search for cases.

1.5 Aim

- Develop an interpretable CAD framework based on the ABCD rules to diagnose skin lesions automatically. The goal is to utilise statistical models to extract each ABCD rule (asymmetry, border, colour, and Dermoscopic structure). Each rule will be trained using individual SVM models and are combined using Bayesian Fusion.

1.6 Objectives

- Develop and validate skin lesion segmentation and border cut-off approach for improved irregularity detection of ABCD rules using SegNet and LBPC.
- Develop and validate melanoma classification based on the diagnostic procedure ABCD rules (asymmetry, border, colour, and dermoscopic structures) for improved interpretability to doctors using various statistical techniques and SVM models.
- Develop and validate combining ABCD rules for the probabilistic analysis of the most dependent features using Bayesian fusion. This could include meta-data for gender, age, touch, feeling, and location on the body.

1.7 Contributions to knowledge

1. **Developing and validating a novel skin lesion segmentation approach for accurate border cut-off segmentation to improve border irregularity analysis using SegNet and LBPC.**

SegNet is highly accurate at finding the area for the segmentation of skin lesions but is inaccurate for measuring border irregularities because the border cut-off between skin and skin lesion is insufficient. Border irregularity detection necessitates an accurate cut-off for more reliable results, which SegNet does not provide. LBPC solves this problem by exaggerating the cut-off and improving the accuracy of border irregularity detection. However, the disadvantage of LBPC is its inaccuracy when finding the skin lesion area. By combining SegNet and LBPC, detecting the skin lesion area using SegNet, followed by adjusting the border with LBPC; retaining the accuracy of SegNet while improving the border cut-off accuracy. Experimental testing utilising the PH² dataset containing expert segmentation data will determine the benefits of segmentation.

2. **Developing and validating a novel asymmetry analysis approach for improved irregular asymmetry detection in skin lesions using moment-based texture analysis for improved bi-fold analysis and superpixels for improved asymmetry colour comparisons.**

The disadvantage of asymmetry measuring techniques for skin lesions is rotational moments for creating bi-folds. Current bi-folds solely consider the silhouette of the skin lesion, with no consideration towards colour or texture. Furthermore, recent techniques have measured asymmetrical irregularities based on colour and texture. Producing a bi-fold based on the shape, colour, and texture using moment-based texture analysis should improve the accuracy of asymmetry detection. In addition, utilising superpixels to measure colour asymmetry to avoid merging important features improves accuracy. Both techniques will be validated using the PH² asymmetrical score.

3. Developing and validating a novel interpretable melanoma classifier for improved interpretability of ABCD rules (asymmetry, border, colour, and dermoscopic structures) using feature extraction, support vector machines (SVM), and Bayesian fusion.

The disadvantage of many neural network-oriented techniques is their lack of adequate interpretability, making them challenging to utilise in clinical environments. However, ABCD rules (asymmetry, border, colour, and dermoscopic structures) are a diagnostic procedure that most doctors are familiar with; therefore, developing a system automating this procedure is beneficial. Feature extraction techniques aim to separate the data essential for each ABCD rule and train an SVM model from the extracted features. For example, bi-folds measure asymmetry, which can be modified to train an SVM model. Repeating this for border, colour, and dermoscopic structures ensures that each rule is independent. Finally, combining the Bayesian fusion results measures the probabilistic significance between ABCD rules and combines them into benign or malignant. Techniques will be validated using the PH² dataset for testing ABCD rules and ISIC 2018 datasets for diagnosis.

4. Developing and validating a novel interpretable melanoma classifier with meta-data including age, gender, feeling, and location on the body to improve classification accuracy between melanoma and seborrhoeic keratosis (SK) using Bayesian probability for a modifiable probabilistic analysis.

Seborrhoeic keratosis (SK) is a melanoma mimic because it sometimes shares clinical features with melanoma. Moreover, differentiating between the two with entirely image data can lead to inaccuracies. Including meta-data age, gender, feeling, and location on the body should improve accuracy because SK appears more frequently on the head or back of old male patients. Bayesian probability networks are considered highly modifiable and can generate results with incomplete input, meaning meta-data is only inputted when necessary, benefiting doctors and improving the diagnosis. The associated organisation has a vast amount of valuable meta-data alongside image data of skin lesions; a private dataset will be created from these results and used to validate results.

Chapter 2

Systematic Review

2.1 Introduction

This chapter reviews statistical and neural network algorithms for the automatic classification of melanoma. Following a discussion on the effectiveness of techniques and whether they are useful within clinical environments.

2.2 Skin Lesions

2.3 Diagnostic Procedures

2.4 CAD Systems for Skin Lesion Diagnosis

2.5 Case-Based Reasoning

2.6 Discussion

Melanoma is a deadly skin cancer that frequently results in the death of patients if develops into metastatic melanoma. This refers to when the cancer has burrowed past the skin and makes its way into blood and internal organs. From this point is it far more difficult to remove.

Melanoma develops from melanocyte cells, which in turn produce melanin resulting in skin pigmentation (brown patch of skin). This means there are visual characteristics of melanoma as it continues to grow. Alongside the necessity to improve the diagnostic accuracy the visual characteristics being ideal for the development of computer vision-based algorithms, this has sparked the creation of algorithms and in turn papers.

When doctors utilize a clinical diagnostic tool they should be capable of rationalising and building explanations based on the data provided from that tool. Currently, many

techniques[7] called named ‘black box’ approaches produce parallel diagnosis that lacks adequate explanations for clinical environments. These provide insufficient information for use within some clinical environments[7]. Instead, it would be beneficial for doctors to follow procedures they are familiar with, such as diagnostic procedures including ABCD rules. The reviewed techniques aim to automate the ABCD rules using various statistical and machine-learning techniques. Many are interpretable and suitable for clinical environments.

Hybrid machine learning techniques are recently gaining traction, an example by Ali combines results from both Gaussian naive Bayes (GNB) and a CNN[4] for border irregularity detection. The CNN ensures high-accuracy classification by finding the relationship between each component, and the GNB is interpretable. Results are combined using an ensemble approach, making a prediction probability. Such techniques are promising for use within clinical environments.

There is a lack of literature describing adequate visual representations for doctors, and it is understandable as there is still little evidence proving that CAD systems improve doctors decision making-processes[32]. It would be beneficial to create literature describing a catalogue of different visualisations that benefit doctors. Putting all this information together, alongside a questionnaire, might provide further insight into the visualisations that might be most useful to doctors.

2.7 Research Methodology

The reason for writing this review was to select the best approaches to skin cancer detection and regarding whether they can be utilised within clinical environments.

Combining the information helps specify what is currently known in literature and highlighting what areas need further work.

Literature is chosen considering techniques that are explainable or have supporting techniques developed for explainability.

2.7.1 Research Questions

The goal of this systematic review is to answer the following questions:

1. What are the major techniques developed for the detection of skin cancer?
2. Are these techniques suitable for use within clinical environments?
3. Can these techniques be supported with other algorithms to improve explainability?

2.7.2 Search Criteria

2.8 Artificial Neural Network (ANN) Techniques

An artificial neural network is a nonlinear statistical prediction technique.

| Search Term | Set of Key Words |
|-------------|------------------------------|
| Skin | skin cancer, skin treatments |

2.9 Convolutional Neural Network (CNN) Techniques

2.10 Deep Neural Network (DNN) Techniques

2.11 Kohonen Self-Organising Neural Network (KNN) Techniques

2.12 Generative Adversarial Network (GAN) Techniques

2.13 Explainability Techniques

The techniques mention in this section are ones including deepshap that are used alongside existing DNN techniques to make models more explainable.

The Local Interpretable Model-agnostic Explanations (LIME)

LIME has been tested in healthcare for the analysis of breast tumor classification[**rafferty2022**], and diagnosis of pigmented skin lesions[**duell2021**]. Its ability to calculate feature importance for machine learning predictions has made it a valuable tool for improving the interpretability of AI models in the medical domain.

2.14 Ensemble Learning Techniques

Ensamble learning is a branch of machine learning based on the decision-making process to intergrate it into systems better[**xu2022**]. Decision-making is the process of making a choice among many options and summarizing evidence to draw a conclusion. An example is case-based reasoning which involves classifying and presenting visually or statistically similar cases and their results.

2.15 Hybrid machine learning techniques

Hybrid machine learning are techniques that aims to use the superior accuracy of deep learning algorithms that are difficult to interpret alongside more explainable algorithms including bayesian networks, SVMs and others. Results are then combined to reach a result.

2.16 Feature Extraction Techniques

Many CAD frameworks follow a methodology for the classification of skin lesions. These are listed below:

1. Segmentation – Image segmentation is the process of partitioning an image into multiple segments for more accessible analysis. These areas can be separated manually by a dermatologist (known as the ground truth) or separated automatically using statistical or machine learning algorithms.
2. Feature Extraction - Gathering features through filtering, morphology and other statistical approaches. ABCD rules include asymmetry, border, colour, and dermoscopic structures.
3. Combination - Combining the extracted features before using Principal Component Analysis (PCA) or after classification using Bayesian Fusion. Others combine the results using the Total Dermoscopy Score (TDS).
4. Classification – Measuring the results from the features and components through classification. Containing the final diagnosis of the type of skin lesion (Naveus, SK, or Melanoma)

2.16.1 Segmentation

Yading Yuan and Yeh Chi Lo describe a fully convolutional network (FCN) with an accuracy of 91.7% with the PH² dataset[47]. FCN is a variation of a CNN using 1x1 convolutions instead of dense layers. Essentially, an FCN forms a more complex function (generating a more complex neural network), whereas the CNN forms a less complex function, likely to degrade essential features. Therefore, more data is needed to train an FCN effectively than a CNN. After the convolution layers, transposed convolution layers (or deconvolution) and other layers (un-pooling) up-sample the input feature map to the size of the input image. Then, the network, trained from ground truth (human-generated segmentation mask) and the original images, can automatically generate segmentation masks based on textures and colours of the skin lesion provided. There are dozens of examples of this, such as SegNet[9], which is another transposed CNN not designed initially for skin lesions but is effective at segmenting skin lesions.

E. Meskini et al. proposed using Otsu binarisation - a threshold technique that is effective at locating the border of a skin lesion after segmenting using Segnet[23]. Researchers proposed that when analysing the skin lesion border using ABCD rules, the original SegNet methods were ineffective because the ground truth is subjective - ineffective at finding the border cut-off between the skin lesion and skin. While SegNet has a 91.7% with the PH² dataset, the data is not effective at finding the precise border cut-off required for accurate border classification using ABCD rules. Therefore, researchers proposed the Otsu

threshold to find the skin lesion border after segmenting using SegNet. Fan proposes another technique that uses a saliency-based segmentation approach to capture the area, followed by an Otsu threshold[15] to find the border cut-off from the skin lesion with a precision of 96.78% validated using the PH² dataset.

Pedro M.M. Pereira et al. proposed local binary pattern clustering (LBPC) to exaggerate the border, producing accurate results when classifying ABCD rules than ground-truth borders in the PH² dataset[28]. Local binary patterns (LBP) are texture descriptors calculated by comparing the centre pixel (of each pixel in the grey scaled image) with the eight neighbouring pixels as 'i', and converting it to a binary using the equation: $[if centroid > neighbour_i = 0, otherwise = 1]$. These eight neighbouring values produce a binary of 01101100 (decimal of 108) and change the centroid to 108. Next, the described process repeats on each other pixel in the image. Finally, the newly filtered image subtracted from the original grey-scaled image creates a segmentation mask with an accurate border cut-off. Finally, Pereira describes classification methods using SVM or FNN presenting the extracted border with an accuracy of 79% and 77% (respectively) with the MED-NODE dataset.

2.16.2 Handcrafted Features

Handcrafted features are the extraction of particular features using statistical algorithms the benefit of separating data into components is a more accessible breakdown, improving explainability. In addition, this might instantiate trust for use within a clinical environment and prove more helpful to doctors.

Asymmetry

Asymmetry can be measured using the bi-fold technique, which involves drawing a line down the middle of the skin lesion and comparing the two halves to confirm whether the sides match, on both the horizontal and vertical axes, as shown in 2.16.2. If the two sides are greatly different, it could be a warning sign of melanoma. Asymmetry can be measured using the shape[48], colour[19], and texture[3].

Measuring the asymmetrical shape requires a precise border cut-off. Ihab S. Zaqout[48] describes a technique using the centroid and rotation of the skin lesion using moments of inertia. By Folding the skin lesion on both vertical and horizontal axes subtracting the opposite half. Pixels that cannot subtract are summed and compared with a threshold considering the skin lesion asymmetrical if the combined sum is more than the threshold.

Reda Kasmi and Karim Mokrani[19] describe creating a grid of 20x20 pixels of the skin lesion image and converting it into the LAB colour space. Next, each block's average colour is compared with a perpendicular block (vertical and horizontal axes) using the three-dimensional Euclidean luminance distance, a-axis, and b-axis. If more than half of the colour comparisons are over the threshold, that axis is considered colour asymmetrical.

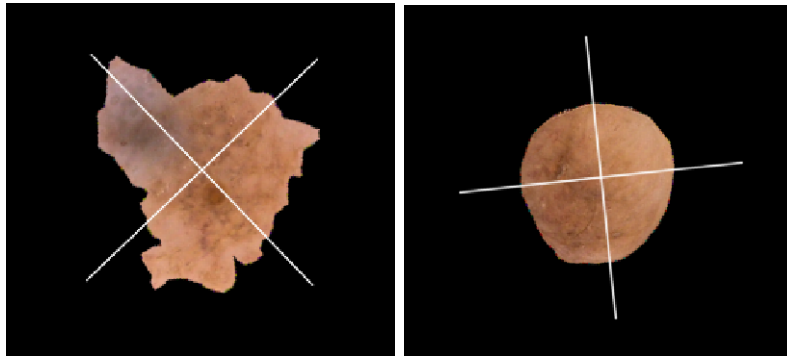


Figure 2.1: Images of two skin lesions from the PH² dataset showing the asymmetry calculated from moments.

Blocks that have no symmetrical pair are ignored. Finally, luminance calculated separately prevents brightness problems. This technique has an accuracy of 94% with a private dataset.

Measuring similarities in texture can be achieved by using SIFT-based similarity and projection profiles[3]. SIFT is scale-invariant and helpful for texture components with varying texture quality. First, the skin lesion is split vertically and horizontally across the centre into four halves, comparing texture components on the symmetrical halves and measuring the similarity. Lastly, the projection profile in the x and y directions generates histograms. These results train a decision tree and have an 80% accuracy of the ISIC 2018 with 204 images privately annotated for ABCD rules and combined.

Border

Estimating border irregularities involves splitting the skin lesion into eight equal sections (through the centroid), where each section with tight corners and convexity is considered irregular. Each irregular section of the border adds a score of 1 ranging from 0 to a total of 8, as shown in figure 2.16.2.

Border irregularity contours were found by splitting the skin lesion into eight segments around the centre, and then calculating a fitting error for each. If the error is larger than 0.05 (x contour), that area is considered irregular[19].

Abder Rahman H. Ali et al. calculate the compactness of each border by first calculating the contour around the area of the lesion containing x and y positions. Next, measure the space between each position to estimate the compactness. The tighter the curves and corners, the more contour positions, revealing irregular borders within a segment, combining all of these scores creates the irregularity index[48].

Fractal dimensions (FDs) is a statistical index measuring the detail in a pattern changing with the image scale index. One technique called box-counting increases values if there are more corners and edges around the border. The higher the value demonstrates the level of

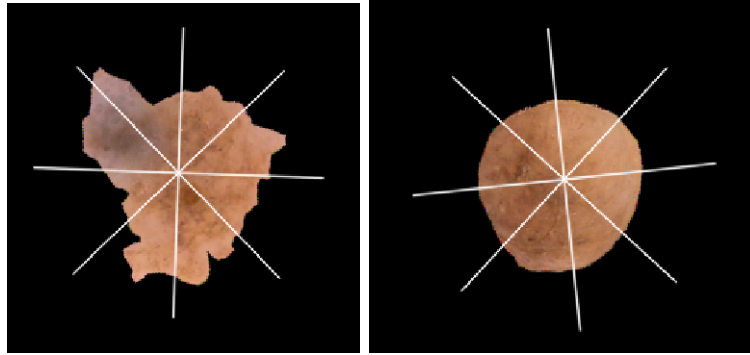


Figure 2.2: Images of two skin lesions split into 8 sections using moments, each border is measured for irregularity.

border irregularity. Ali describes using machine learning alongside Zernike moments, and convexity measurements for a high-accuracy border irregularity classification[4]. However, results are ambiguous because the output is either “irregular” or “regular” border (not relating to the TDS). Thus, conforming to the TDS and splitting the border into eight sections would make it more interpretable and useful o doctors. However, a hybrid GNB and CNN approach are combined to allow interpretability through GNB.

Colour

Colour refers to the shades of pigment within the area of a skin lesion, not referring to abnormalities relating to bruises, crust, and grazes. Melanoma usually contains more than two colours compared with benign lesions, singular in colour. Skin lesions can consist of one or many colours: white, red, light brown, dark brown, blue-grey and black.

Finding colour variations has been achieved by calculating the normalised standard deviation of the red, green, and blue components[35]. The normalisation process improves the recognition of normal skin pigmentation, which would show pigmentation levels, making comparisons easier between different skin lesions.

Arthur Tenenhaus, et al. utilise joint learning using Kohonen map, and k-means clustering[41]. Five random pixels create a 5 by 5 Kohonen map represented by 25 neurons in a neural network for each skin lesion in the dataset. Colour variations on a 25-dimensional vector find the proportions of pixels projected onto each of the 25 neurons. Next, K-means classifies the skin lesions set by the number of colours found by dermatologists. Only four colours were present in the dataset in this scenario, while seven could be. Eventually, the colour components are represented as a 42-dimensional vector and are passed into a KL-PLS based classifier to detect variations in colour at 66% using a private dataset.

Reda Kasmi, et al. locate the number of colour variations by converting the image into the LAB colour space matching the colour ranges that can be perceived by human eyes[26],

measuring the average colour distribution of the dataset and assigning each colour as a threshold range. Next, the Euclidean distance between each colour threshold is compared with each pixel colour[19], finding the closest matching colour of the six colours. Finally, removing the areas of colour with less than 5% prevents the classification of dots. This approach uses a colour range of white, light brown and dark brown. However, there is a static threshold value for the other colours, which would be unlikely to cover the ranges of the colours, including red, blue-grey, and black.

Dermoscopic structures

Dermoscopic structure refers to structures on the skin lesion, including pigment networks, structureless areas, dots, globules, streaks, white structures, and 22 others (not including sub-types). Variations of pigment networks are more commonly found in melanoma[6] and are therefore a valuable feature for automatic classification. Similarity other features such as milia-like cysts, a sub-type called milia-like cysts (MLC) called cloudy MLC appears more frequently on melanoma than SK, with a specificity of 99.1% specificity[37].

Javier López-Labraca et al.[22] describes a statistical approach to classifying melanoma using dermoscopic structures through Gabor filtering, support vector machines, and Bayesian fusion. This technique uses a form of soft segmentation to find the area of these dermoscopic features. Firstly the structures are located using Gabor filtering using different values to find fissures and globules. Each structure is then compared with a trained SVM model to check the similarity of the detected features. The results from the model are then combined using Bayesian fusion to reach a result of malignant or benign. Finally, training a CNN model alongside an SVM improves the retractability of dermoscopic structures; compared to a standalone CNN model.

2.16.3 Combining ABCD Rules

This section describes combining features from the ABCD rules into a classification between malignant, suspicious or benign after considering all clinical features. Again, meta-data and texture can potentially improve the results.

Maryam Ramezani et al. proposed a method to extract features from ABCD rules storing them in vectors and extracting the texture as a GLCM. First, these 187 features are shrunk to 13 using PCA[29]. Next, the data trains an SVM to classify skin lesions into benign or malignant with an accuracy of 82.2% on macroscopic images using a private dataset.

Other methods output TDS[48, 49], which combines them using: $[(\text{Asymmetry} \times 1.3) + (\text{Border} \times 0.1) + (\text{Colour} \times 0.5) + (\text{Diameter} \times 0.5)]$. A statistical model for each ABCD rule outputs a score in the same format. The benefit is interpretability because it follows the diagnostic procedure. The technique achieved an accuracy of 90% using a private dataset.

2.17 Datasets

2.18 Challenges of Explainability

2.19 Conclusion and Future Work

Many techniques utilise ABCD rules to produce an automatic and interpretable diagnosis. Interestingly, many focus on detecting and classifying asymmetry, border, and colour (ABC) or dermoscopic structures, but neither combine the whole ABCD rules into a single framework. Despite dermoscopic structures providing a means of diagnosing problematic forms of melanoma, including mimics (seborrheic keratosis)[18], and non-pigmented melanomas. Thus, it would be valuable to combine both into a single system for possibly higher accuracy.

Despite various valuable features, asymmetry rarely utilises techniques other than statistical models. For example, researchers highly focused on border irregularity and dermoscopic structures, leading to hybrid machine-learning models for their assessment. However, asymmetry still utilises statistical approaches to measure and combine shape, colour, and texture. It would be beneficial to transform this data and process it using an SVM, improving accuracy.

Utilising external data, including feeling, touch, age, and location on the body, are helpful to doctors when diagnosing skin conditions, but is not mentioned in any of the discussed techniques. It would be beneficial to implement this data into the decision-making process.

Chapter 3

Dataset Suitability for Melanoma Detection

3.1 Introduction

This chapter contains an analysis of some popular datasets including ISIC 2019, and PH2. The goal is to identify any relationships between skin lesions and patients. Using this analysis ‘the dataset’ is created using NHS macroscopic images and metadata.

There is an analysis of the distribution of metadata in these datasets, discussing whether they are consistent with the literature. For example, SK is more likely to have milia-like cysts compared to melanoma. So we check if the distribution of data in datasets specifies this. The reasoning for this is that a Bayesian network is used later and trained on datasets based on the distribution of data. Therefore ensuring that the data is scientifically relevant ensures the Bayesian network is functioning correctly. Certain criteria are found to be ineffective and removed because they are not consistent with the literature.

3.2 Other Datasets

The analysis of skin lesions is an especially laboured field, so there are a huge number of relevant datasets to discuss. Public datasets include MEDLINE, PH2, ISIC, and others making a total of 21 open-access datasets containing 106,950 skin lesion images[**Wen2022**]. Out of these datasets, only the PH2 dataset has publicly accessible metadata regarding ABCD rules with a total of 200 images. ISIC is the largest of these datasets, being a combination of many other datasets, with extra annotations from the original.

The datasets listed in table3.2 include the number of images, classes, and metadata. Out of these datasets ISIC 2019, PH2 and 7-Point Criteria appear to be the most promising. PH2 is especially useful because it is the only dataset representing ABCD rules on asymmetry and colour. SKINL2 was considered, but ISIC 2019 was a much larger dataset with more

| Name | Year | Image Type | Number | Classes | Metadata |
|------------------|------|---------------------------|--------|---------|--|
| ISIC 2019 | 2019 | Dermoscopic | 33,569 | 8 | Age, anatomical site, gender, and diagnosis |
| PH2 | 2013 | Dermoscopic | 200 | 3 | Asymmetry, colour, pigment network, dots/globules, streaks, regression areas, blue-whitish veil |
| MED-NODE | 2015 | Macroscopic | 170 | 2 | n/a |
| SD-198 | 2016 | Dermoscopic & Macroscopic | 6,584 | 198 | anatomical site, symptoms, duration, morphology, and colour |
| SKINL2 | 2019 | Macroscopic (unique tool) | 376 | 8 | Gender, age, and fototype |
| 7-point Criteria | 2018 | Dermoscopic & Macroscopic | 2000 | 2 | Pigment network, regression, pigmentation, blue-whitish veil vascular structures, streaks, dots/globules |

Table 3.1

metadata. SD-198 is publicly available but not accessible.

Overall ISIC 2019 and PH2 are the most suitable datasets. The PH2 dataset is utilised for an analysis of feature extraction techniques such as the detection of ABCD rules and dermoscopic structures. Then the entire technique is analysed using the ISIC 2019 dataset, which is the largest public dataset.

3.3 Issues

One fundamental problem is the overutilisation of private or privately annotated datasets, making a direct comparison of algorithms (especially relating to ABCD rules) difficult. Some are between benign and malignant[23, 19, 4, 3] while others utilise private or never mention any datasets[19, 35, 41, 29, 48]. None compare their ABCD rules, likely because of subjectivity depending on the dermatologists that labelled them. Ideally, more datasets and labels should be public to assess individual rules and reach objective measurements. Until then, testing algorithms conform with malignant, suspicious, or benign. This is especially true for the PH2 dataset, although it was around before some of these publications it was not used for testing.

Although there is an ISIC 2020 dataset with a total of 44,108 images, its diagnosis is between benign and malignant and other metadata is on atypical melanocytic proliferation, café au lait macule, lentigo NOS, lichenoid keratosis, naevus, seborrheic keratosis, solar lentigo, and other/unknown. The metadata is very specific and doesn't match the requirements of the project, so ISIC 2019 is still a better candidate.

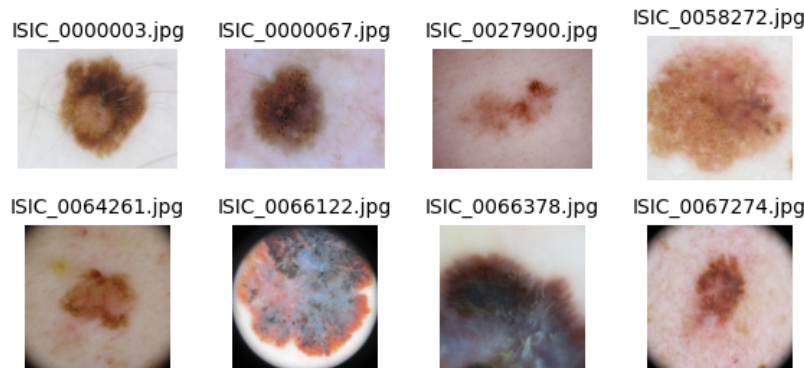


Figure 3.1: Examples from the ISIC 2019 dataset, where first two images are BN, followed by two SK, and four MM.

| Name | Year | Total Samples | Differences |
|-----------|------------|---------------|---|
| HAM10000 | 2018 | 11,526 | n/a |
| BCN 20000 | 2016 | 19,424 | Includes nails and mucosa |
| MSK | 2015, 2017 | 3918 | Coloured stickers covering un-applicable skin lesions |

Table 3.2

3.3.1 ISIC

The ISIC dataset is a collaborative effort of many institutions to support the development of automatic classification methods for melanoma detection. The most recent applicable dataset is ISIC 2019, which contains a total of 25,331 images for training and 8,238 for testing, making 33,569 images in total. Each image has corresponding metadata including sex, age, anatomical site, and diagnosis. These images are separated into classes melanoma (MM), melanocytic nevus (MV), basal cell carcinoma (BCC), actinic keratosis (AC), benign keratosis (BC), dermatofibroma (DF), vascular lesions (VL), and squamous cell carcinoma (SCC). This includes segmentation masks.

Images in the dataset shown in figure 3.3.1 are captured with a dermoscope and making it substantial for analysing the structures of the skin lesion. However, many of the lesions have incomplete borders, which is especially true for MM because of its increased size to other lesions. It would be a good idea to detect and remove samples that do not have a complete border when analysing ABCD rules.

ISIC 2019 is a combined source of data from different hospital datasets including HAM10000, BCN 20000, and MSK described in more detail in table 3.3.1. This is important to mention because each dataset has images captured with differing diagnostic procedures resulting in varying resolutions and styles in which the images are taken. MSK includes coloured stickers covering un-applicable skin lesions that are within the area of the image

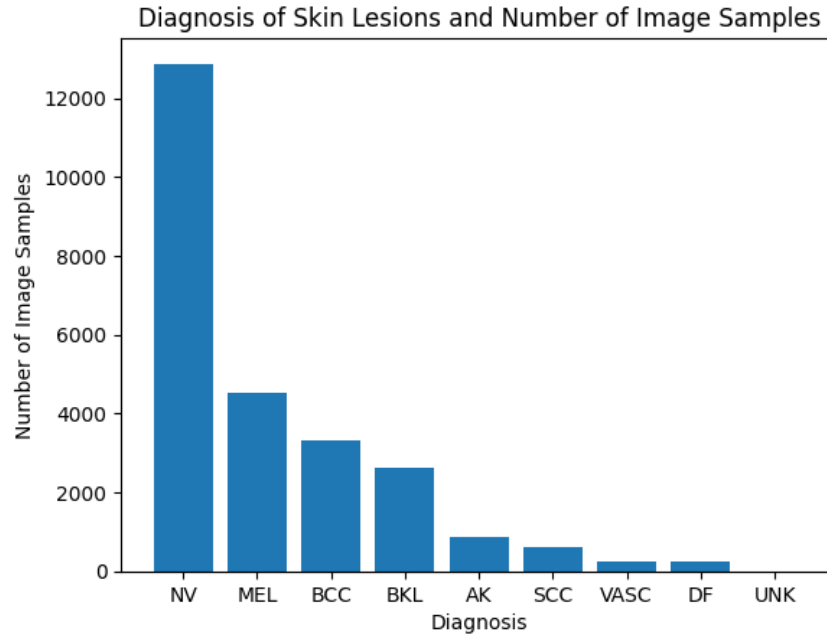


Figure 3.2: ISIC 2019 dataset showing the number of image samples and the diagnosis of those skin lesions dataset appears to be highly unbalanced with half being NV.

and the camera appears to be further away. BCN 20000 contains rarer types of images including nails and mucosa, which do not appear in the other datasets. HAM10000 does not appear to have any notable differences, but it is still captured with different tools and resolutions.

As demonstrated in figure3.3.1 the dataset is highly in-balanced based on the diagnosis of the skin lesion with 12,875 NV and 4,522 MEL. There are only 867 AK, where AK has a very high variance compared to other skin lesions and the sample size is unlikely for adequate detection. Seborrheic keratosis (SK) is not in this dataset and AK a similar lesion is described instead. There are only a handful of images for DF, and VASC. The difference in image samples makes the dataset primarily useful for testing between NV and MEL.

Metadata

In this dataset, the images are accompanied by metadata describing patient information. This includes patients age, sex, and anatomical location. Analysing this data provides further insight into the influence of patient information on the classification process. Most of all we are looking for similar numbers for each category and some cases might be removed to balance the dataset and improve classification results.

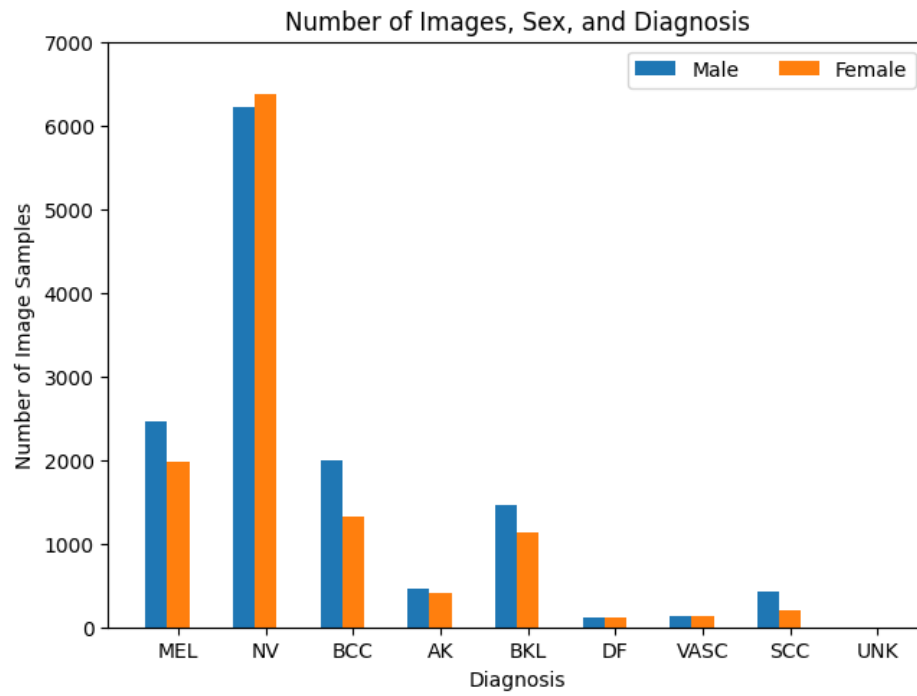


Figure 3.3: The dataset has more male than female patients except for NV which has more samples.

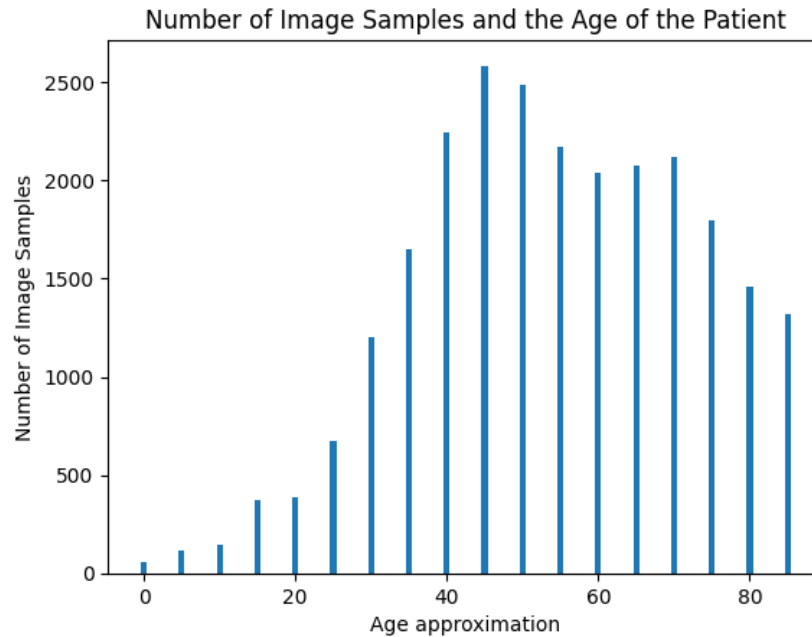


Figure 3.4: This shows the number of image samples compared to the age, the dataset is largely unbalanced regarding age where patients are between 40 and 75 years of age.

Figure3.3.1 demonstrates the number of samples relating to the patient's sex. There are more samples for each type of skin lesion except for NV which there are slightly more female samples. They are all within a very close range and are unlikely to need rebalancing.

As demonstrated in figure3.3.1 the dataset is unbalanced relating to age and type of skin lesion. Variation is likely a result of skin lesions being more likely to develop in older people than younger ones. This might mean that many of the skin lesions are developed and there is going to be unlikely to find underdeveloped skin lesion samples.

In figure3.3.1 the age approximation (in intervals of 5) was compared with the diagnosis. The black line (whisker) represents the minimum and maximum range of age, the box (quartile) shows the interquartile range (IQR), and the centre line in the middle represents the median. Some dots represent outliers in the data, that are outside the age range.

Each class in the diagram is a diagnosis associated with the age of each patient. Interestingly, represented in this data SCC, BCC, and AK appear to develop more in older adults with a median of age 70. Many younger patients were diagnosed with NV with a median age of 46. Whilst MM appears to be diagnosed in adults with a median age of 60. This is correct when regarding literature[empty citation].

The comparison between diagnosis and anatomical location provides further insight into the variety of samples. Figure3.3.1 demonstrates the percentage of image samples (based on

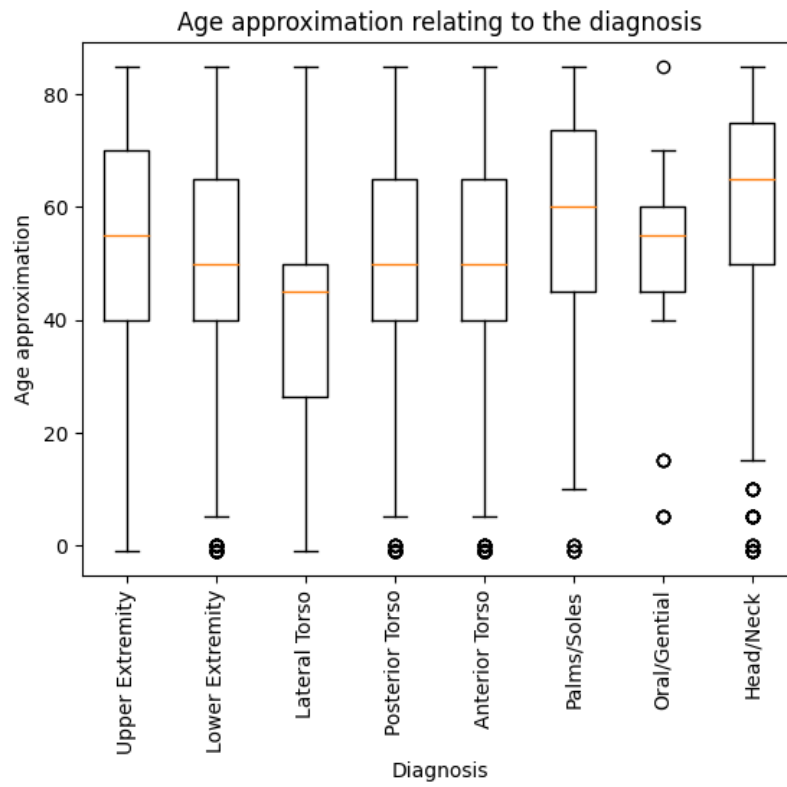


Figure 3.5: The approximate age range of patients and their diagnosis.

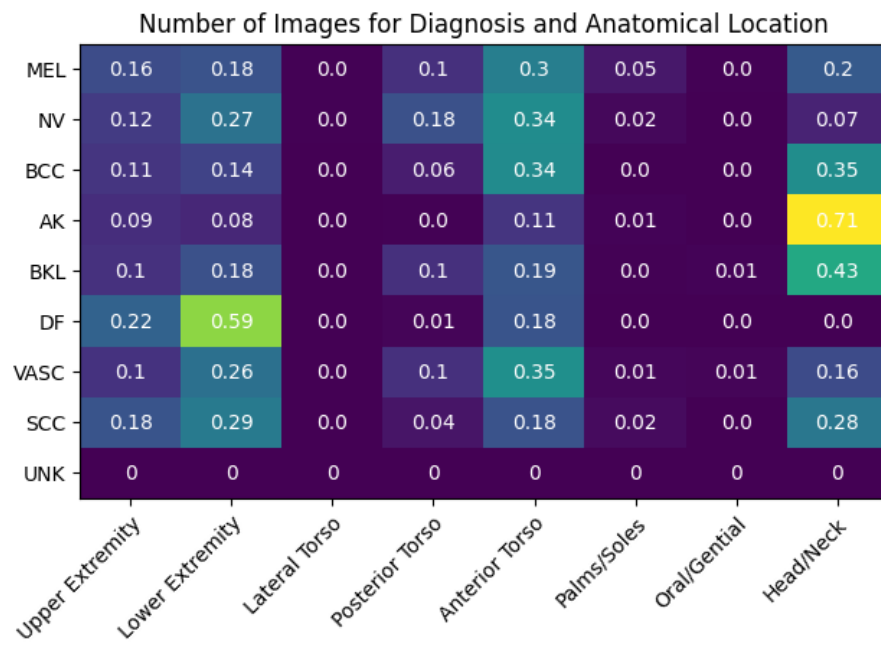


Figure 3.6: Shows image examples associated with the anatomical location and age of the patients.

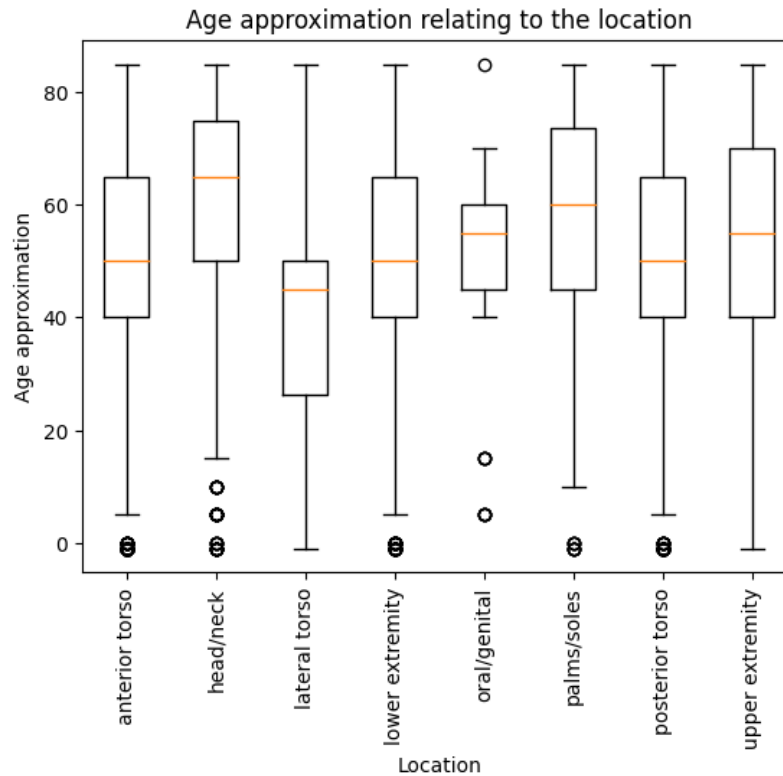


Figure 3.7: Shows image examples associated with the anatomical location and age of the patients.

the diagnosis) there are for diagnosis and anatomical location. Interestingly, AK appears on 69% of images on the head/neck. So there is a strong likelihood that skin lesions are overlapping facial features. Furthermore, DF appears more on the lower extremity and upper extremity at 58% and 22% respectively. Both AK and DF are consistent with the literature[empty citation].

Another interesting finding is that most skin lesions are in areas of the body that are frequently exposed to the sun, being anterior torso, head/neck, and lower extremities.

Figure3.3.1 is similar to3.3.1, except it compares the approximate age and location of the skin lesion. There are more older patients who have been diagnosed with skin lesions on their head/neck and younger for the lateral torso. It is concerning that there is a distinct lack of younger patients for palms/soles and head/neck, which could mean more developed skin lesions in these criteria.

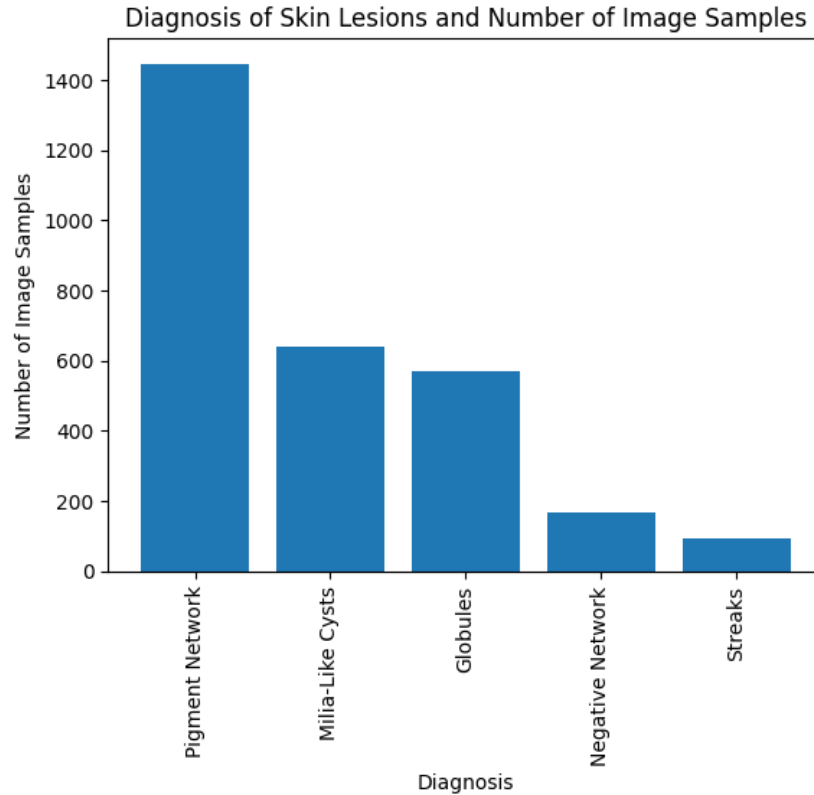


Figure 3.8: Number of images containing dermoscopic structures.

Dermoscopic Structures

ISIC 2017 shares some images with ISIC 2018 including some additional metadata relating to dermoscopic structure. This includes 2,694 segmentation masks of pigment networks, negative networks, globules, milia-like cysts, and streaks. While the original in ISIC 2017 only has metadata for dermoscopic structures, it was linked to ISIC 2018 using image file names to get their diagnosis. The diagnosis is only between benign naevi, seborrheic keratosis, and melanoma.

The dermoscopic structures described in figure3.3.1 show the number of image samples for each dermoscopic structure. Naturally pigmented networks have more than 1400 images which makes it ideal for training a SegNet algorithm. Other dermoscopic structures are lacking, such as streaks has less than 100 images. This is too small for most machine learning algorithms.

As described in figure3.3.1 certain dermoscopic structures are split almost evenly between melanoma and benign naevi, except for streaks and negative networks being more common.

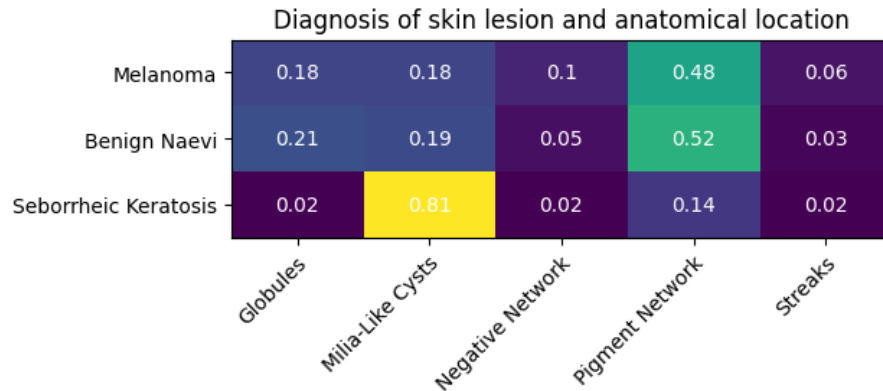


Figure 3.9: Number of dermoscopic structures relating

This demonstrates the importance of being able to detect the difference between typical and atypical pigmented networks. Furthermore, milia-like cysts appear more frequently in seborrheic keratosis and there is a lack of pigmented networks. These are again consistent with literature.

Summary

In summary, the ISIC dataset including data from 2017, 2018, and 2019 makes this dataset the largest public dataset for skin lesion analysis and melanoma detection. It contains a large collection of dermoscopic images with 8 different diagnoses. The dataset having 33,569 makes it ideal for a diverse range of research and development purposes including the evaluation of machine learning and deep learning models. It also contains 2694 images of dermoscopic structures labelled in the ISIC 2017 version of the dataset. Overall, this is the best dataset currently publicly available for the analysis of skin lesions.

Furthermore, data distribution comparing diagnosis to the age, anatomical location, and dermoscopic structures appears to be consistent with literature[empty citation], likely due to the size of the dataset. Otherwise, some image samples have incomplete borders. So, some images should be detected and removed to properly utilise asymmetry, border, and colour.

3.3.2 PH2

The PH2 dataset is a collection of dermoscopic images that were made available in 2013 by Mendonca, et al[empty citation]. It consists of 200 images including 80 common nevus, 80 atypical nevus, and 40 Melanoma. Although the dataset is small it holds substantial metadata for describing features within the skin lesion, including asymmetry, colour, pigment network, dots/globules, streaks, regression areas, and blue-whitish veil. This is the only

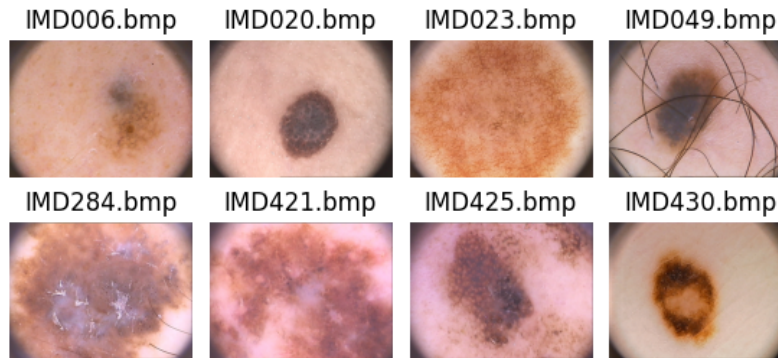


Figure 3.10: Example of images from the PH2 dataset. The first two are standard, the second two are atypical, and the last 4 are melanoma.

dataset that has such substantial data regarding the mentioned features. Each image has a segmentation mask of the skin lesion.

The images in figureph2-example-images are some examples of skin lesions from the PH2 dataset. All the images have a circular border and melanoma samples are too big to fit inside the area of the dermoscope in many cases. This results in incomplete border making it difficult to analyse asymmetry and border from ABCD rules.

As shown in figure3.3.2 there are 200 image samples in total with 80 common nevus, 80 atypical and 40 melanoma. The number of image samples is too small for most neural network techniques. The dataset is highly unbalanced with only 40 melanoma images and 160 naevus images. With such a skewed distribution of classes, the model might become overly biased towards the majority class (naevus), leading to poor performance in identifying melanoma. Another issue is the size of these classes, the scarcity of samples will likely result in overfitting when training models. For this reason, this is not a reliable candidate for training machine learning algorithms when considering that more diverse candidates such as ISIC exist.

Metadata

The benefit of this dataset is the rich metadata allowing for the analysis of specific features within an image and the relationship between them. This allows for the development of more sophisticated algorithms that provide further insight into the characteristics of melanoma and naevus.

Demonstrated in figure3.3.2 demonstrates there is substantial data for measuring the asymmetry score based on the total dermoscopy score (TDS). Typically the algorithms used to measure asymmetry such as bi-fold do not require any training, making the smaller sample size ideal. However, there is a very small sample size for both TDS of 1 and 2, and

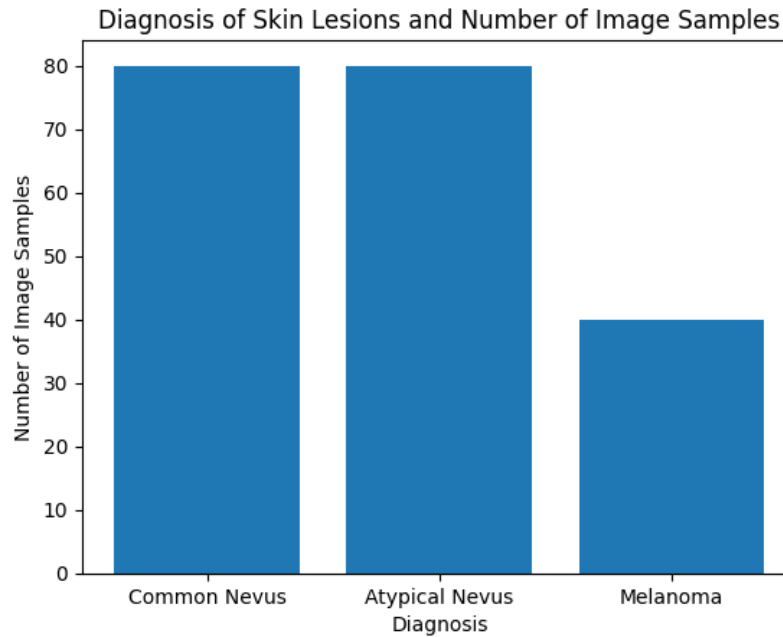


Figure 3.11: Number of image samples and diagnosis in the PH2 dataset.

it would be beneficial to have more.

The observation in figure3.3.2 shows the percentage of images associated with each colour. Light and dark brown are commonly associated with typical naevus. On the other hand, white, blue, and black are more common in melanoma that indicate structural and vascular irregularities. This is true to literature where melanoma is more likely to have a range of colours. The scarcity of red samples demonstrates that it is uncommon in nevus and melanoma. Red is certainly more common in melanoma, but with only a sample size of only 9 the data is likely too stunted to demonstrate this. Other lesions including BCC are more likely to contain red[empty citation], but these lesions are not included in this dataset.

There are many records of pigment networks, and dots/globules, but as seen in Figure3.3.2 there are roughly 20 samples for each streaks, regression, and blue-whitish veil. The data is highly unbalanced, so it will be difficult to train a machine-learning algorithm for these features. There are more samples of pigment networks, and dots/globules because common. For this reason, typical and atypical features are a good indication of whether the skin lesion is melanoma.

Figure3.3.2 shows dermoscopic structure labels relating to the diagnosis of the skin lesions. Common nevus have typical and present dermoscopic structures, atypical nevus have just as many absent with more present and atypical. Melanoma has more present and

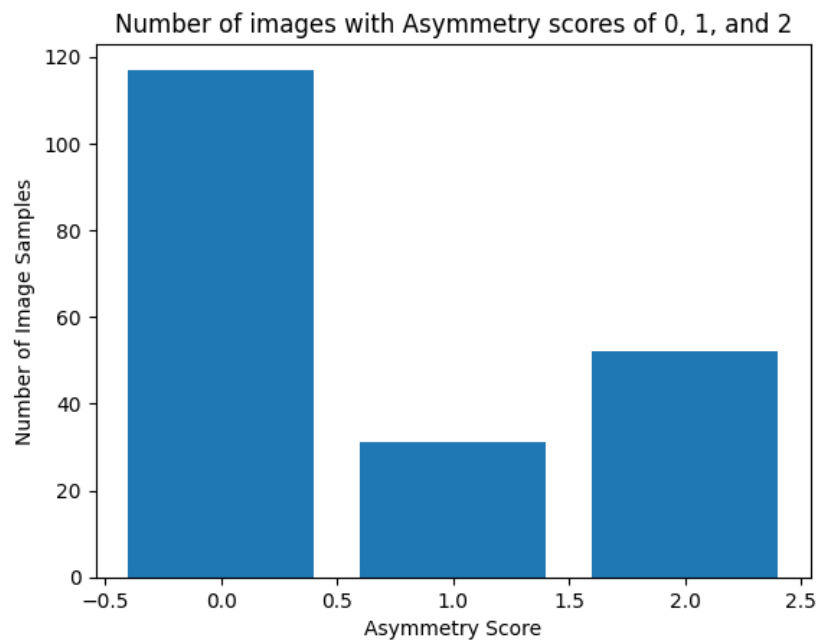


Figure 3.12: This shows the number of image samples and asymmetry score based on Total dermoscopy score (TDS).

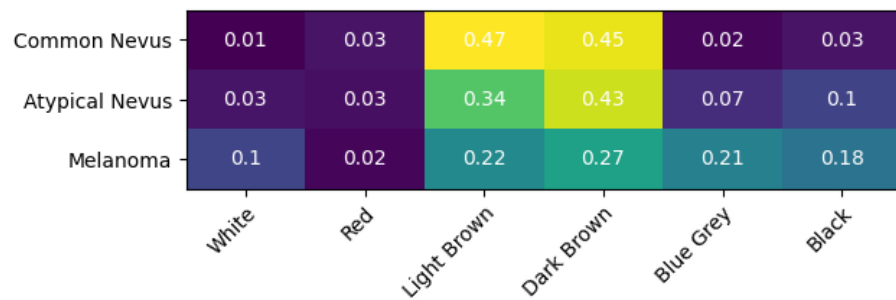


Figure 3.13: Number of colours in the PH2 dataset compared with the diagnosis. Colours are in order white, red, light brown, dark brown, blue-gray, and black.

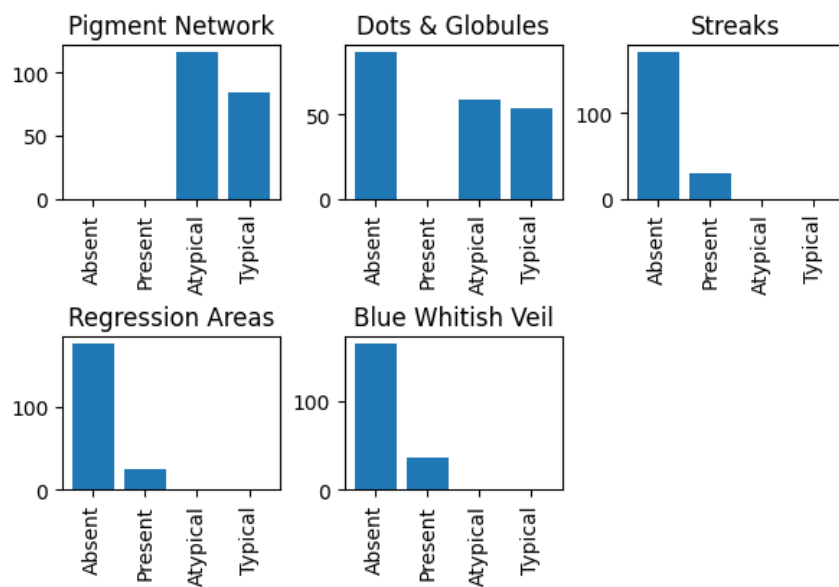


Figure 3.14: Dermoscopic structures and the number of images. These are labelled between absent, atypical, present, and Typical.

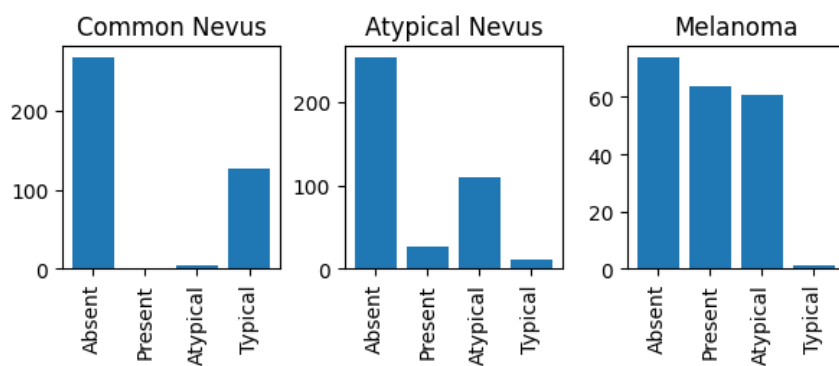


Figure 3.15: Shows the labels of dermoscopic structures, number of images, and diagnosis. These are labelled between absent, atypical, present, and Typical.

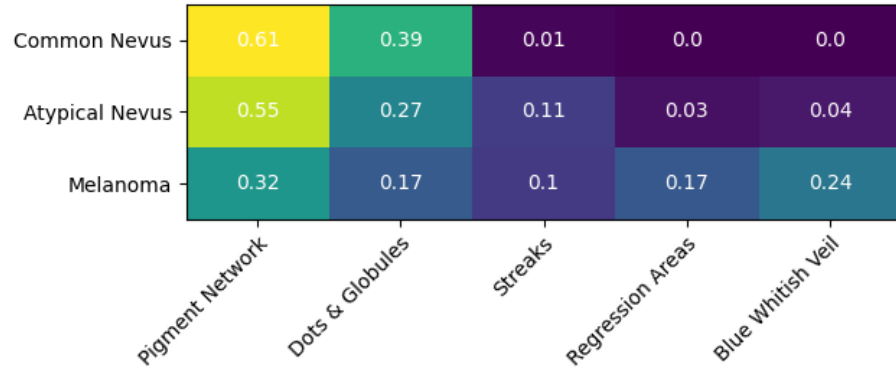


Figure 3.16: Shows the number of images based on the diagnosis and dermoscopic structures present, typical, and atypical.

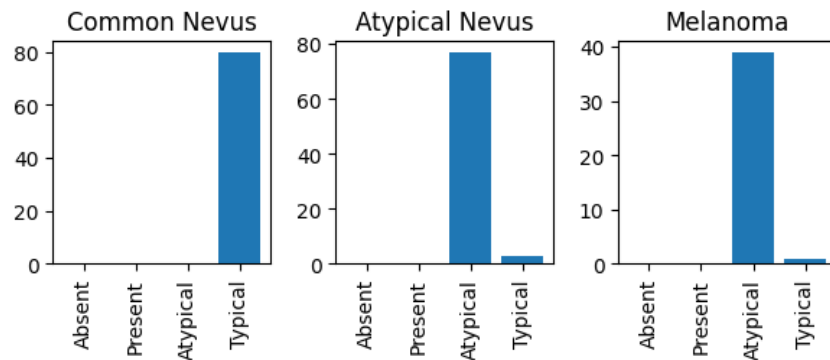


Figure 3.17: Pigment network data relating to the diagnosis.

atypical types of skin lesions.

Figure 3.3.2 demonstrates that pigment networks are present in both nevus and melanoma. Furthermore, streaks, regression areas, and blue-whitish veils are more common in melanoma. Pigment networks and dots/globules use different labels of typical and atypical so it is understandable they do not change between lesion types.

There is little to no overlap between typical and atypical pigment networks between melanoma and naevus. Shown in figure 3.3.2 common naevus are all typical pigment networks, while atypical naevus and melanoma are labelled atypical. This demonstrates that testing for pigment networks should be on type (typical and atypical) instead of whether they are present. Unusually, there is very little overlapping in the data. This is very unusual unless it was designed this way purposely, but it would have been more useful to have more samples without pigment networks.

3.3.3 Diagnosis and Image Assessment

Summary

In summary, the PH2 dataset is a valuable resource for researchers considering it is the only one of its kind to provide metadata relating to asymmetry, colour, and dermoscopic structures. This has been used frequently in various studies to develop and evaluate algorithms for skin lesion analysis. Such datasets with substantial metadata are useful for producing explainable results. As explainable (XAI) becomes more common datasets describing clinical features will be necessary. However, one of the downfalls of this dataset is the unusual labelling for dermoscopic structures where the pigment network and globules are labelled between typical and atypical and others are between present and absent. Some metadata was inconsistent with literature including the colour red, which is more common for melanoma, but the data does not demonstrate this. Furthermore, almost every image sample has a pigment network (although common), it would be more useful to have some without this feature.

An issue with this dataset is that many of the papers that utilise ABCD rules and dermoscopic structures do not test their algorithms against this dataset, regardless of the dataset being around before the time of publication[19, 35, 41, 29, 48]. Instead they tend to use privately annotated datasets, which makes it difficult to replicate results. After analysing PH2 dataset it is likely the small size, lack of red colour samples and the unusual labelling of dermoscopic structures are the reason for this dataset being avoided. Furthermore, the ABCD rules tend to be subjective and are only relevant to the institution which they are used, therefore this is likely again why the technique is being avoided and why many papers tend to annotate their own data. Hopefully some time in the future objective measurements can be accepted and datasets including vast data like PH2 will be accepted.

3.4 Conclusion

Overall both the PH2 and ISIC 2019 provide adequate data for the testing and developing algorithms. ISIC 2019 is suitable for training deep learning algorithms with a total sample size of 33,569 images with relevant metadata. PH2 is certainly the weakest link with data samples of only 200 images between benign naevi and moles and that many papers refuse to test using the dataset and resort to privately annotating their own data. Regardless PH2 appears to be suitable for analysis apart from the lack of red samples.

Considering the data distribution of the dataset both samples appear to be consistent with literature. For example in ISIC 2017 dermoscopic structures, SK has more samples with milia-like cysts and less pigment networks. Furthermore melanoma and benign naevi have roughly equal pigment networks and less milia-like cysts. Another example is the colour distribution in PH2 while brown and light brown are common in benign naevi, MM has less samples of light and dark brown with more colours of blue, black, and white. The

only sample that appeared to be wrong was the colour red, where there was a severe lack of samples.

3.5 Developing the NHS dataset

Whilst recognising the benefits of the ISIC 2019 and PH2 datasets we can begin to develop ‘the dataset’ using NHS data. The inclusion of NHS data brings real-world clinical cases into the mix, and techniques developed during this project can be tested in the scenario it is intended to be utilised.

Requirements are decided below to highlight potential biases and issues, and then 2,000 images are chosen to create the dataset. This is followed by an analysis similar to the previous datasets and interesting findings from the data.

3.5.1 Requirements

The use of machine learning algorithms for the detection of melanoma is a promising and evolving field with detection accuracies often beating that of dermatologists[7]. However, the effectiveness of such depends heavily on the quality of the datasets used to develop them[38]. The goal of this section is to describe and document the data extraction process from the National Health Service (NHS) and highlight biases, pre-processing, and other potential issues involved in the training of machine learning algorithms for the detection of melanoma. Requirements are first highlighted before gathering the data and are listed below.

There are requirements for this project, which include the use of macroscopic images instead of dermoscopic images. Macroscopic is described as viewing with the naked eye or by taking a picture with standard lenses. When referring to Dermoscopic images, are images captured with a specialised tool called a dermoscope that removes lighting variegation and improves the visual features within the skin lesion usually called dermoscopic features.

Although macroscopic images are used it is important to note that dermoscopy improves the diagnostic accuracy of dermatologists for melanoma when compared with macroscopic examination[46] and is widely considered superior[42]. Dermoscopic images provide a detailed visualization of patterns and structures on the surface of the skin lesion that might not be visible to the naked eye[42]. Some of these structures are pigment networks, asymmetry, irregular borders, and other features that support the differentiation between benign and malignant lesions[42].

Another example shows the diagnosis for BCC was 91% when using dermoscopy, compared to 57% when using close-up images[13]. Similarly, the sensitivity for SCC was 77% with dermoscopy, compared to 70% with close-up images[13]. These findings highlight the superior diagnostic performance of dermoscopy compared to macroscopic.

The dermoscopic examination is superior to macroscopic examination, however, the project use case specifies macroscopic. The logic behind this is that the tool is specifically

designed for general practitioners who are unlikely to recognize dermoscopic features, so there is no need to supply them with dermoscopes. This appears to be consistent with an author's findings showing that 92% of dermatologists correctly recognize at least four size types of melanoma. In contrast, only 38% of non-dermatologists were able to recognize the same number of melanomas[38]. Therefore, 'the dataset' is created with macroscopic images for examination.

Considering the use of macroscopic images there needs to be a more thorough clean-up of the data for it to be used effectively. This will include removing hair and specular reflections to improve classification accuracy. This chapter will discuss the data transformation of NHS macroscopic images, including augmentation techniques to remove lighting, hair and other anomalous data from the images. All of which will support improving the accuracy when classifying.

3.5.2 Data Biases

The use of datasets is fundamental to the development and evaluation of machine learning algorithms, and the accuracy and effectiveness heavily weigh on the quality of the data used. Biases can arise from data collection procedures and pre-processing techniques. Not considering possible biases greatly affects machine learning algorithms using them and their effectiveness. Furthermore, careful consideration is essential to ensure the accuracy and reliability of the conclusions proposed in this document. Failure to consider all these factors could result in skewed conclusions that could undermine the validity of findings. For these reasons, it is essential to carefully identify and evaluate data before using and testing it.

NHS datasets contain a wealth of information that can be utilised. However, some biases need consideration before creating a dataset. These biases include:

1. The diagnostic procedure dismisses skin lesions without recognizably suspicious features and does not reach the phase that photographs were captured. As such, there is a lack of typical benign skin lesions within the dataset, and most have some undesirable features.
2. Dermatologists and general practitioners have diagnosed the large majority of skin lesions which have varying accuracy depending on their experience. Images include metadata on the department and person capturing the image, so the doctors' experience can be measured.
3. Dermatologists could diagnose during an in-person examination where patients can be asked questions in real-time and further tests can be made involving touch. Otherwise, dermatologists diagnose using previously saved images, which might be less accurate because they lack the insight that an in-person examination would provide.
4. Some skin lesions within the dataset lack metadata including their diagnosis. Such image samples should be avoided.

5. Diagnoses of skin lesions are written in plain text including question marks where there is some uncertainty and the possibility of multiple diagnoses. Only diagnoses that are certain of their findings are used.
6. Photographs of the skin lesions may be captured on different body parts such as hands, legs, face, and others. Most pre-processing methods are designed to differentiate between skin and skin lesions, so it is important to avoid using these images. Otherwise, new pre-processing methods will have to be made and tested.
7. Seborrhoeic keratosis (SK) has similar features to that seen in malignant skin lesions. Therefore, there might be skin lesions diagnosed as melanoma that are SK. Furthermore, because of its similarity, there are many SK images. It will be vital to separate these.

Following the potential issues 2,500 images were chosen from the NHS database. Eight types of skin lesions were chosen Malignant Melanoma (MM), Seborrhoeic keratosis (SK), Atypical Naevi (AN), Benign Naevi (BN), Squamous Cell Carcinoma (SCC), and Basal Cell Carcinoma (BCC).

1. Malignant Melanoma (MM): A type of skin cancer that arises from melanocytes, which are responsible for the pigment melanin (brown skin).
2. Seborrhoeic Keratosis (SK): A non-cancerous growth that originates from cells called keratinocytes.
3. Atypical Naevi (AN): This refers to an unusual or atypical mole that shares characteristics of skin cancer, but they are not cancerous themselves
4. Benign Naevi (BN): Normal benign mole that most people have.
5. Squamous Cell Carcinoma (TM): A form of skin cancer that develops from squamous cells in the outer layer of skin.
6. Basal Cell Carcinoma (BCC): The most common type of skin cancer, that develops from basal cells located in the outer layer of skin.

The database system where the skin lesion images were located uses fotoware software. While there are a substantial number of images roughly reaching 20,000, these were obtained using diverse methods including dermoscopic and macroscopic. Other issues included and were removed:

1. Dermoscopic (Not used in this study)
2. Duplicates (keeping one)

3. Skin lesions were not visible
4. Abnormalities, edge of an ear or belly button
5. Angled or far away images
6. More than 2 skin lesions
7. Almost entirely covered with hair
8. Tattoo
9. Scars
10. Incision

Some images were angled and far away which made it hard to get a clear view of the skin lesion. Others contained multiple skin lesions making it difficult to differentiate which one was being diagnosed. Others including tattoos and incisions were considered more extreme cases and deliberately excluded because there were not enough samples or outside the criteria of the project, respectively.

To remove the mentioned samples a search criteria was used, the example below is for finding melanoma:

("01 Close-up " -"Dermoscopy" -"eye lid" -ear -Nose -scalp -lip -cheek - scar -toe) AND
(-SCC -BCC -"Seb k" melanoma -"atypical mole" -mole)

Some samples could not be removed automatically so they were removed manually by looking through the images. After finding all the samples, the following

1. BN = 500 (600)
2. AN = 500 (600)
3. MM = 400 (500)
4. SK = 200 (264)
5. BCC = 200 (300)
6. SCC = 200 (203)

A significant difference between this and other datasets is the inclusion of benign naevi and atypical naevi. An atypical mole is an unusual naevi that has features similar to cancer but is non-cancerous. This will provide further insight into their distinguishing characteristics and into the difficulty of diagnosing atypical naevi from other skin lesions.

In the next section, further analysis of the images using the metadata will be conducted to remove image samples with uncertain diagnoses and to balance the dataset for better use with machine learning algorithms.

| Attribute | Description |
|----------------|--|
| Image ID | an integer representing the image ID - example: 123456.xxx |
| Doctor | a string representing the forename and surname of the doctor that made the diagnosis - example: JOHN SMITH |
| Department | a string representing the name of the department - example: DERMATOLOGY |
| Studio | a string representing the name of the studio used to capture an image of the skin lesion |
| Capture date | an integer representing the date the image was captured - example: 00:00:0000 |
| Hospital ID | a string representing the hospital ID |
| Gender | a string representing patient gender |
| Date of Birth | an integer representing patient date of birth - example: 00-00-0000 |
| Surname | a string representing patient surname |
| Forename | a string representing patient forename |
| Initials | a string representing patient initials |
| Patient ID | an integer representing patient ID |
| Subject (Tags) | an array representing method the image capturing method (Dermo or Close-Up) and anatomical location |
| Creator | a string representing the forename and surname of the photographer - example: JOHN SMITH |

Table 3.3: This table shows the metadata in each image and a description of each label. Rows highlighted in red are removed to protect patient confidentiality.

3.6 Data Transformation and Analysis

Each image holds metadata shown in table 3.6 as EXIF Tags within each image. After extracting the images the metadata included in the images are Filename, Tags (Capturing method, anatomical location), Gender, DOB, Department, Consent, Historical Diagnosis, Diagnosis, and Date Photographed. There was other metadata with each image, but they are potentially identifiable, so to protect patient confidentiality, they were removed.

This is a generalised diagnosis, alongside these images are historical diagnoses of the skin lesion, written in plain text in some cases this question marks when the doctor is uncertain of a diagnosis and other times it includes a slash and a different diagnosis. Although it is not a specific format making it difficult to process, it includes a wealth of knowledge.

3.6.1 Historical Diagnosis of Skin lesions

The historical diagnosis is written text by the doctor that includes the possible diagnosis. The format is dependent on the doctor, so it changes dramatically. Generally, this is a '?' to show uncertainty and a '/' followed by another diagnosis. All of the variations in the format are shown in table 3.6.1.

Some historical diagnoses contain a '?' showing uncertainty from the doctor. Figure 3.6.1 describes the number of skin lesions between uncertain and certain. Interestingly AN, BN,

| Image ID | Historical Diagnosis |
|-------------|---|
| 998444.jpg | SEB K |
| 549982.JPG | AK / SCC |
| 824466.jpg | ATYPICAL MOLE / ? MM |
| 879067.jpg | ? ATYPICAL NAEVI |
| 1028628.jpg | ? MM / ? BCC |
| 154414.jpg | 1) ? SCC 2) SBCC 3) ? SPOT |
| 739199.JPG | (1) BOWEN'S DISEASE (2) SUPERFICIAL BCC |
| 586010.JPG | SUSPECTED N. MM |

Table 3.4: Examples of historical diagnosis and doctors and some unique variations of labelling.

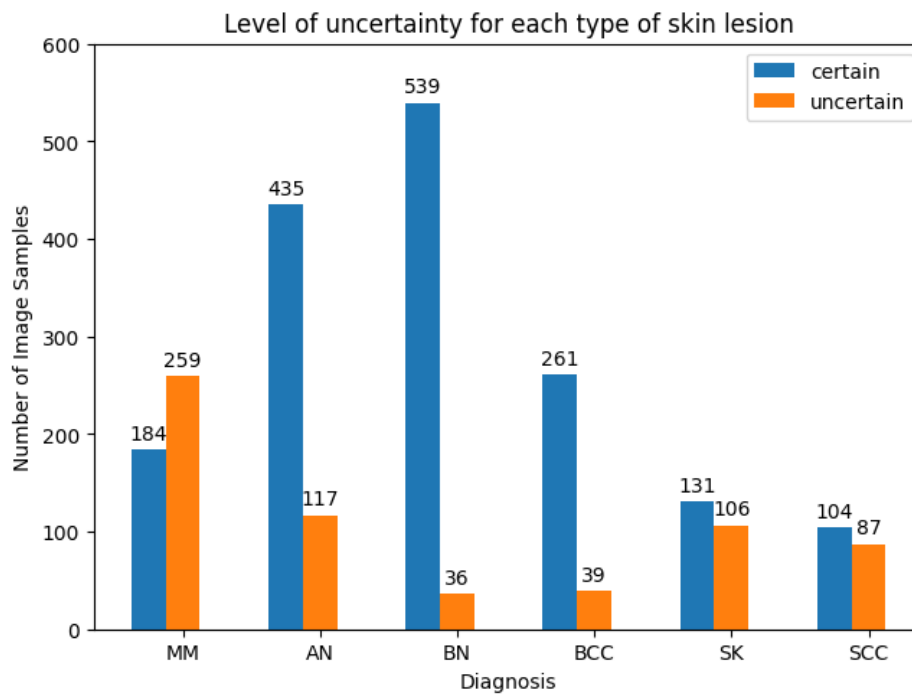


Figure 3.18: Number of image samples relating to the historical diagnosis. Labelled as uncertain if there is a '?' in the diagnosis.

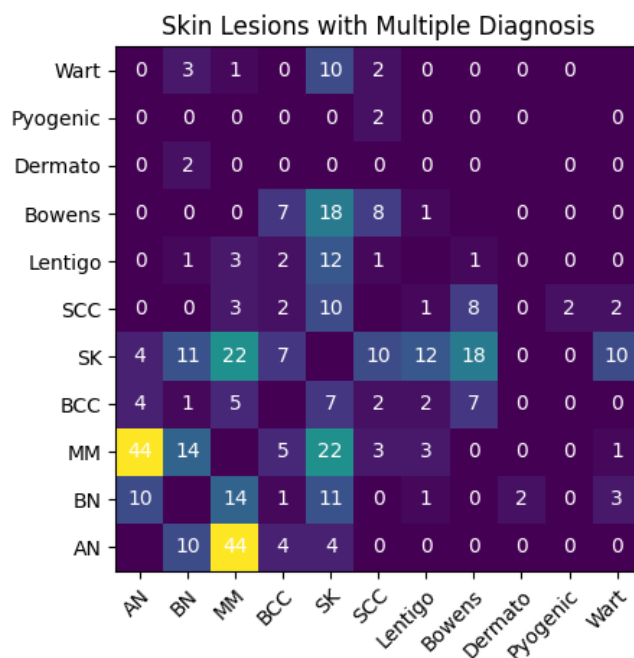


Figure 3.19: Number of skin lesion samples with multiple diagnoses in the historical diagnoses. Other types including lentigo, Bowen’s disease, dermatofibroma, pyogenic granuloma, and wart are only associated with the main diagnoses (AN, BN, MM, SCC, BCC) because they are not specifically searched for. This means they are only found in association with the mentioned main diagnoses and this data is likely missing data comparing the other types.

and BCC appear to be certain with 117, 36, and 39 respectively. Followed by SK and SCC are roughly half of the images at 106 and 87. Most of all MM shows that more than half of the diagnoses at 259 are uncertain out of 184 that are certain. This in turn demonstrates the type of skin lesions that doctors are having difficulty diagnosing where melanoma is especially difficult.

Multiple diagnoses are sometimes shown, figure3.6.1 shows the number of skin lesions with multiple diagnoses mentioned in the historical diagnoses. Interestingly the most commonly associated are AN with MM at 44 and SK with MM at 22 images. Others are SK with MM, Bowen’s disease, lentigo, warts, and SCC demonstrating that SK is associated with the widest range of skin lesions and the difficulty diagnosing it.

Considering that SK has multiple diagnoses mostly for MM and SK, it is a good idea to compare these images and see whether there are any distinguishing features. Demonstrated in figure3.6.1 SK border and colours change dramatically between different lesions demonstrating how difficult it is telling them apart[empty citation]. The ABCD rules and TDS is assigned to each image to see whether this diagnostic procedure will be suitable

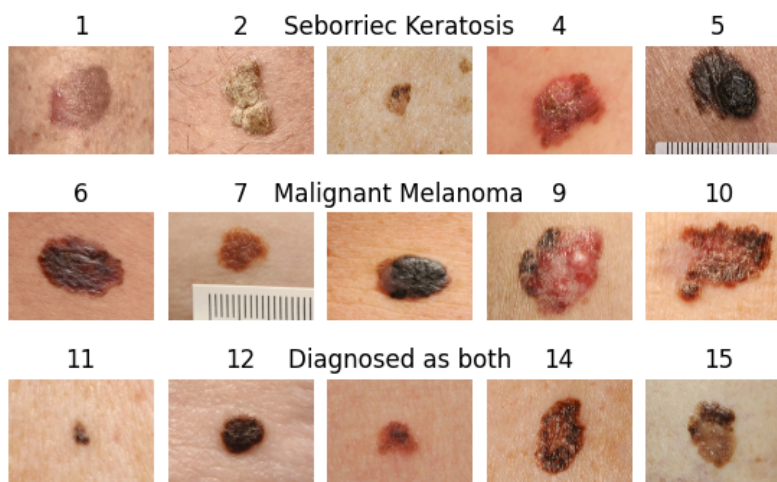


Figure 3.20: Comparing skin lesions that are diagnosed as MM, SK, and considered both MM and SK.

for separating these skin lesions.

3.6.2 Anatomical location

Anatomical location has a total of 28 different descriptors for specific body parts including leg, wrist, neck, etc. To make comparisons easier with the ISIC dataset each label has been assigned to specific areas such as upper extremity, anterior torso, etc. All the locations are listed in the table 3.6.2.

| Category | Organised sub-labels |
|-----------------|--|
| Upper Extremity | Wrist, Elbow, Arm |
| Lower Extremity | Leg, Knee, Hip, Ankle |
| Lateral Torso | Axilla, Breast |
| Posterior Torso | Back, Shoulder |
| Anterior Torso | Chest, Abdomen, Trunk |
| Palms/Soles | Hand, Thumb, Foot |
| Oral/Genital | Groin, Genitalia, Sacrum, Buttocks, Sacrum |
| Head/Neck | Neck, Chin, Face, Temple, Head, Forehead |

Table 3.5: All the different labelling for the anatomical location of the lesion. Each label in the NHS data has been assigned to a category similar to the ISIC dataset.

3.7 Data Transformation and Augmentation

As mentioned in the data biases section the skin lesion images are taken under various conditions including angles, lighting, and distance from the skin lesion. While the variety of conditions will decrease the accuracy of results and hinder the detection of dermoscopic features, it is a requirement of the project.

One of the main challenges in melanoma detection is the visual similarity between normal and infected regions. Others are the presence of artefacts such as bubbles, hair and clinical marks[2]. These factors lead to low accuracy rates in traditional approaches. However, segmentation techniques can help overcome these challenges by removing these areas and isolating the melanoma from the rest of the image.

Skin lesion augmentation is especially vital because of the use of macroscopic images instead of dermoscopic images. This means there are various artefacts including hair, specular reflections, rulers, varying sizes, and shapes of the skin lesion. All of these can obscure the skin lesion and affect the accuracy of segmentation[Unver2019] and in effect feature detection.

By augmenting the skin lesion images using specular reflection removal and hair removal, the accuracy of feature classification methods can be improved[kasmi2023].

3.7.1 Hair Removal

Hair artefacts in images can interfere with the recognition of handcrafted features and affect the performance of deep learning algorithms in melanoma detection[kasmi2023]. Applying morphological operations such as image sharpening and segmentation techniques can remove hair artefacts from dermoscopic images[kasmi2023].

Dull-Razor is an algorithm developed by Lee et al[Lee1997] and is frequently implemented with

Sharp-Razor[kasmi2023] is a technique for detecting hair and ruler marks to remove them from images. This uses a multiple-filter approach including grayscale plane modification, hair enhancement, segmentation using tri-directional gradients, and multiple filters for hair of varying widths. This technique is shown to outperform existing methods.

3.7.2 Specular Removal

Specular reflection removal techniques are effective in improving the accuracy of melanoma detection[Shen2009]. A technique was proposed utilizing a partial differential equation to iteratively erode the specular component, removing the specular reflection[Shen2009].

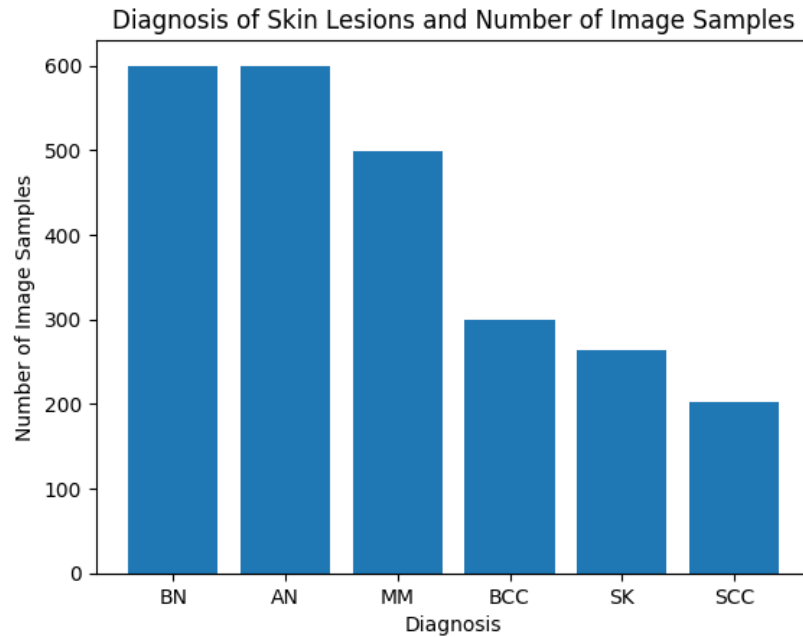


Figure 3.21: Number of image samples relating to the diagnosis of the image.

3.8 Conclusion

3.9 Dataset Statistics

The dataset has been analysed and modified accordingly, originally starting with a total of 2,500 images and it has been amended to 2,271.

As shown in figure3.9 the image data and diagnosis of the skin lesion there are several differences in this dataset compared with the ones described so far. There has been more of an attempt to balance the data so there are more equal samples of each. Furthermore, benign naevi have been split into benign naevi (BN) and atypical naevi (AN). There are images of seborrheic keratosis, which is more than any other public dataset currently available.

The age variation of patients described in figure3.9 demonstrates there are many younger patients included in the NHS dataset. This is substantially different from other datasets including ISIC that have mostly older patients. This demonstrates that there is an influx of younger patients regardless of them not being within the age group where melanoma usually develops. In both ISIC and NHS datasets the median the median is 60 years.

As shown in figure3.9 describing the location of the skin lesions and several image samples. There are more samples on the posterior torso (back) compared with other skin

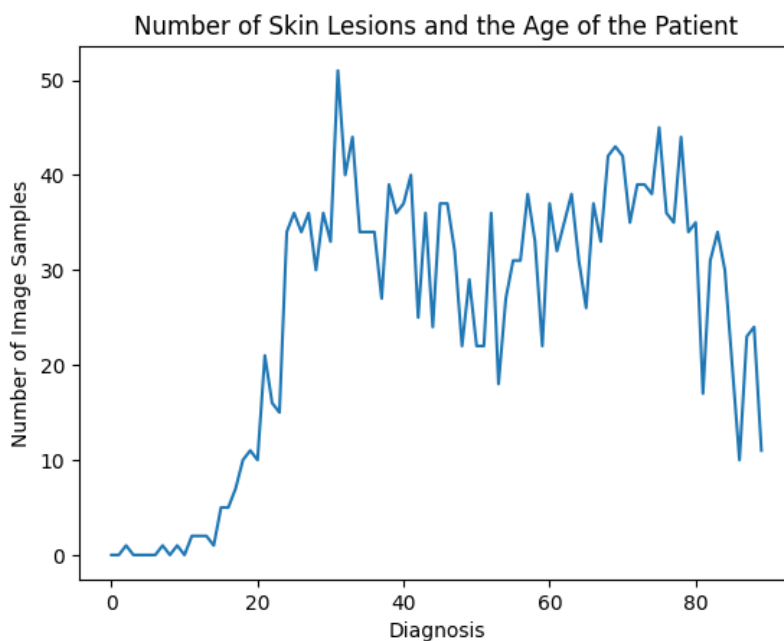


Figure 3.22: Age of patients and number of image samples.

lesions with any of the others. There are only a couple of samples for lateral, palms/soles, and oral/genital. This data was originally modified because it had a total of 28 descriptors, so they were grouped into 8 similar to the ISIC dataset. This can be seen in more detail in figure3.6.2.

Figure3.9 describes the number of image samples relating to the diagnosis and sex of the patients. Interestingly there are almost double the number of female patients being diagnosed for AN and BN compared with MM where there are slightly more male patients and BCC where there is almost double male.

Image samples described in figure3.9 demonstrate the age of patients compared with their diagnosis. Understandably, AN and BN which are neavus are from younger patients, while SK, SCC, and BCC appear in older adults. MM is primarily from patients at the age of 50 to 70.

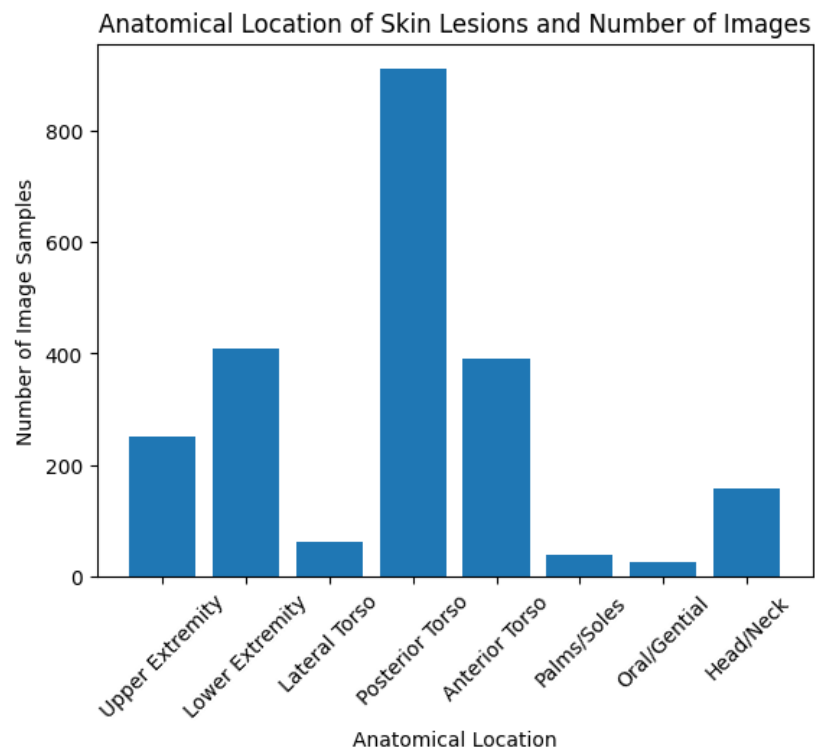


Figure 3.23: Number of image samples related to the location of the skin lesion.

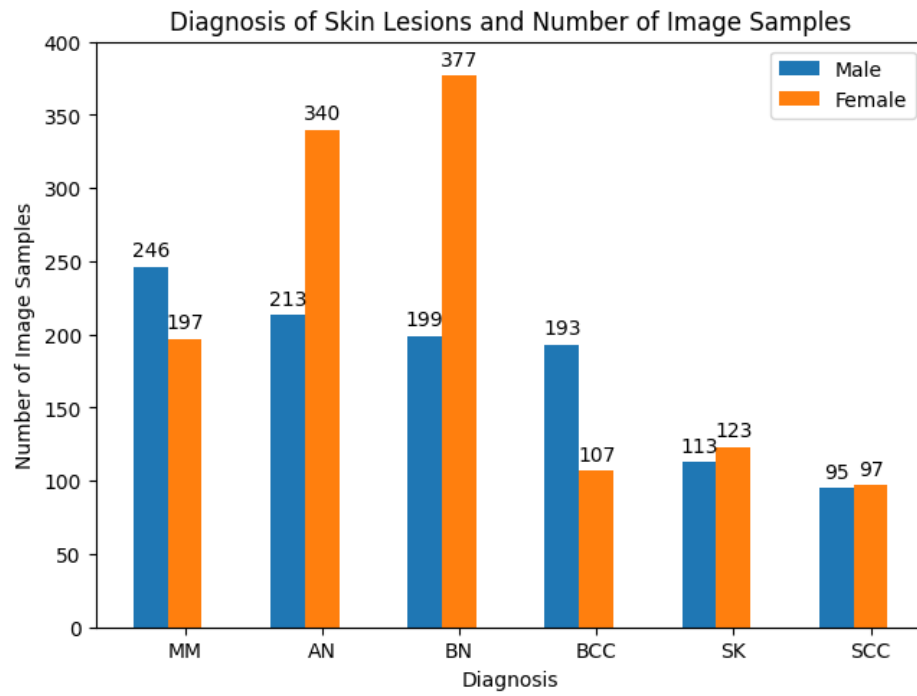


Figure 3.24: Number of image samples relating to the diagnosis and sex of the patients. There are more female than male patients.

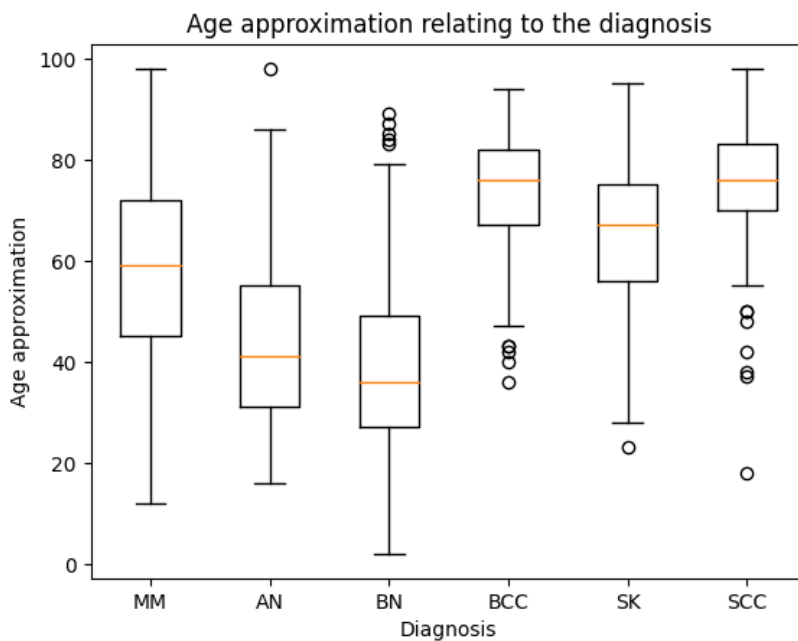


Figure 3.25: Boxplot describing the age of patients and the diagnosis.

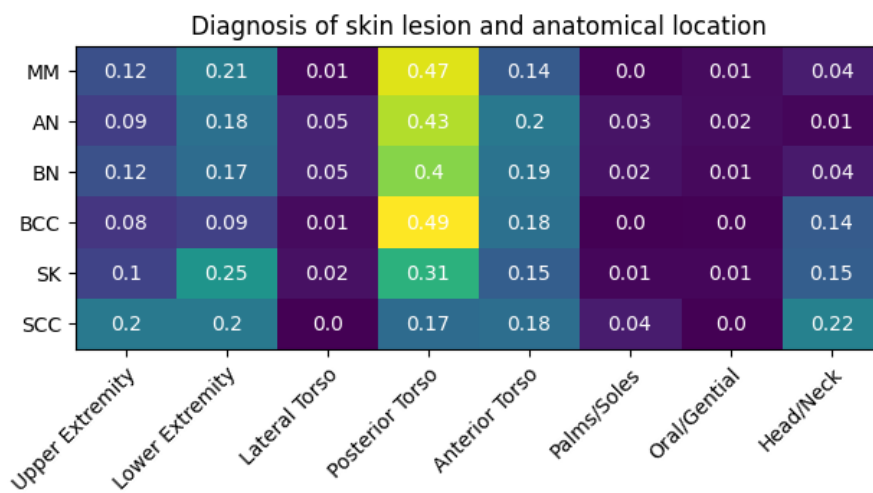


Figure 3.26: Number of image samples relating to the diagnosis of the image.

Chapter 4

Analysis of Explainability for the Detection of Melanoma

4.1 Introduction

This chapter contains an analysis of popular explainable AI (XAI) techniques called DeepSHAP and Gradcam. These techniques were compared to discuss whether their results are interpretable.

4.2 Background

Explainable AI (XAI) has gained significant attention in recent years because of increasingly more complex machine learning models in high-stakes decision-making processes in domains including healthcare, education, and public policy[**amann2020**, **hemphill2023**, **dennehy2023**, **ploug2021**, **wachter2017**]. This issue was highlighted by the General Data Protection Regulation (GDPR and ISO/IEC 27001) has mentioned the concern for machine learning algorithms, mentioning the difficulty of implementation in the medical domain without adequate explanations[**empty citation**]. The public also has a preference for explainable systems??. Transparency, accountability and privacy are the most critical AI ethical principles[**khan2022**] and they must be considered for use within sensitive domains including healthcare.

The lack of explainability in AI systems makes it difficult to evaluate the trustworthiness of algorithmic decisions, especially for the public and experts with little understanding of AI[**dennehy2023**]. Issues could often arise with algorithms relating to data biases, such as the significant lack of data representing darker skin tones[**rizvi2022**]. Without clinicians having an understanding of these issues, they might be misled into using incorrect diagnoses. This also highlights difficulty regarding accountability and whether the AI system or clinician would be blamed for any mishaps. Alongside this, there is a concern for parallel

diagnoses[**empty citation**]. This refers to AI systems that produce only a diagnosis with little to no explanation. Without an explanation, the clinician cannot learn and attempt to understand why the results were met and in turn cannot utilise them. Considering the nature of clinical environments and that people’s lives are at risk, algorithms need to produce explanations so that clinicians can interpret and learn from results, but not depend on them.

Since highlighting the concerns of AI systems progress has been made in developing neural network architectures that are more interpretable. Techniques have since been developed to function with existing machine learning algorithms[16, 34, 31]. This is beneficial because many DNN architectures are the highest accuracy currently available[**empty citation**]. Other techniques[**empty citation**] involve extracting clinically relevant features such as ABCD rules or dermoscopic structures, followed by combining results into a diagnosis. Other issues with these techniques are the current scepticism on whether these techniques are trustworthy[43, 33], and the concern they produce realistic but incorrect results[17]. Techniques such as LIME have been for use within

Some studies have described the use of explainable AI (XAI) models in healthcare[**empty citation**]. One of which shows that the confidence of clinicians is improved.

Lack of interpretability of AI systems has been identified as a challenge and these approaches are commonly referred to as “black box” approaches. This is because their inner workings are not visible and the system is

Some other interpretable techniques do not utilise neural networks. For example, Javier López-Labraca et al.[22] described an interpretable technique using multiple SVM models with colour and three dermoscopic structures (i.e., pigment networks, globules, and streaks). Bayesian fusion combines each model to calculate a diagnosis. Bayesian probability is a type of probability theory that uses probability distribution to estimate the values of unobserved variables. Bayesian fusion has comparable accuracy to neural network techniques[40]. Overall, results should be partially interpretable for use within clinical environments.

4.2.1 Dataset

Comparisons were made using the ISIC 2019 dataset because it is the largest and most robust public dataset currently available regarding melanoma detection.

4.3 DeepSHAP

DeepSHAP (Shapley Additive exPlanations) is a method designed to offer insights into the decision-making process of machine learning models, specifically deep neural networks (DNN). DeepSHAP is an extension of the DeepLIFT algorithm and is based on the concept of Shapley values that are derived from cooperative game theory. The method aims to estimate the importance of input features for a given decision by comparing the activations

in the network for a given input against the activations caused by a reference input. In Turn, DeepSHAP is particularly effective

The method is particularly effective for explaining the performance of deep learning models in medical decision support systems[**empty citation**]. It has been shown to highlight information relevant to the decision-making process. This is more effective than layer-wise relevance propagation (LRP), local interpretable model-agnostic explanations (LIME), and DeepLIFT.

In the field of healthcare, DeepSHAP is applied to predict and explain non-communicable diseases (NCDs). In explanations for individual predictions and a case study detecting the progression of Alzheimer's.

Although explainable algorithms have seen some use within healthcare, there is no evidence of their current use within dermatology.

DeepSHAP (Shapley Additive exPlanations) is a game theoretic approach designed to explain models during training by visualising features related to the classification. It explains the individual predictions in machine learning models using Shapley values that measure the contribution of each feature to the contribution of an outcome[**Aas2021**].

4.3.1 Summary

4.4 Grad-Cam

4.4.1 Summary

4.4.2 Tree ensemble methods

4.5 Bayesian Network Approach

4.6 Conclusion

Chapter 5

Implementation of segmentation, ABCD rules and Dermoscopic structures

5.1 Introduction

This chapter is a discussion of the most popular ABCD (Asymmetry, Border, Colour, and Dermoscopic Features) algorithms including their implementation, and updating the algorithms. They are compared using the PH2 dataset and updated relating to their accuracy.

Surprisingly, many of these techniques were originally on whether they effectively find melanoma and not individual features. So, this will be the first time some of these techniques were tested and documented regarding the ABCD rules.

5.2 Hybrid Melanoma Segmentation Algorithms using Neural Networks and Statistical Models

Segmentation plays a crucial role in melanoma detection because it separates melanoma from healthy skin. Accurate segmentation is essential for various aspects of melanoma diagnosis, treatment, and classification[2] including improving the detection of ABCD rules[**Lee2020**]. This is especially important for border analysis[28, 20] that relies on the analysis of convex and indents. The irregularity of borders is a key feature in distinguishing melanoma from benign lesions, and exact identification of irregular borders from melanoma skin lesions is clinically significant[**patil2021**].

There are various deep learning approaches[2] and deep CNN techniques[**yu2017**]. These highlight the significance of advanced technologies for accurate segmentation and detection

Figure 5.1: Some images from the ISIC dataset demonstrating the difference between segmentation masks and expert segmentation masks.

of melanoma. Although these techniques are massively accurate they are trained using datasets (ISIC 2019) contain rough segmentation masks, resulting in the produced borders having a poor border cut-off. This can be seen further in figure 5.1. This is largely due to ISIC datasets only having a few expert borders and not enough to train deep learning algorithms. Furthermore, the images are also shrunk as part of the deep learning process, which in turn loses smaller features that are of significant when analysing borders. All of this results in the major technologies including deep learning are ineffective when producing border cut-off.

A range of traditional segmentation techniques including SegNet, U-net methods have been shown to outperform other approaches in capturing the most significant melanoma characteristics. However, these techniques do not provide an effective border for the analysis of ABCD rules. Various statistical algorithms have been explored including active contouring-based segmentation[30], LBPC and others for border adjustment including u-otsu and edge-imfill.

5.2.1 Related Works

An approach by Albanhli[2] uses a deep learning-based segmentation algorithm using YOLOv4-DarkNet and active contouring for melanoma and skin lesion detection and segmentation. This technique provides a classification of the skin lesion and a segmentation, demonstrating a high level of practicality for clinical decision support systems.

Seeja R D[seeja2019] proposed a technique that utilizes a convolutional neural network (CNN) based on a U-net model architecture for the segmentation based on colour, texture and shapes. The U-net model architecture is a popular choice for image segmentation tasks due to its ability to capture both local and global features effectively.

Hyunju Lee[Lee2020] proposed a technique that utilizes an edge fill method called u-otsu for segmentation, using the U channel from the YUV colour space to calculate the histogram. Otsu calculates the optimal threshold value to separate foreground and background pixels based on the histogram of the image.

Another technique by Pedro[28] uses a newly developed technique called Local Binary Patterns Clustering (LBPC). Using a Local Binary Pattern (LBP) filter by subtracting the gray-scale image from the LBP filter after a Gaussian filter, resulting in the creation of a mask. This has been successfully used for the detection of melanoma.

5.2.2 Semantic Pixel Wise Segmentation (SegNet)

SegNet is a deep learning architecture that is used for semantic image segmentation for melanoma detection. It was originally developed by [11] and has shown promising results in various segmentation tasks.

The idea of SegNet is to perform pixel-wise classification by assigning each pixel in an image to a specific class or category. This is achieved through a fully convolutional neural network (FCN) architecture, which allows for end-to-end learning and inference at the pixel level.

Semantic pixel-wise segmentation (SegNet) is a machine learning architecture utilizing a deep, fully convolutional neural network (DCNN). This network requires training from ground truth and pre-segmented images for automatic segmentation. SegNet consists of encoding layers, decoding layers, and a pixel-wise classification layer. The encoder layers consist of 3×3 convolutions (including batch normalization and ReLU), and pre-trained filters for classifying features. After some convolutions, the data is down-sampled using a 2×2 pooling layer. Next, decoding layers consist of up-sampling, followed by 3×3 convolutions. Finally, the pixel-wise classification uses a softmax layer to represent each pixel between 0 and 1 based on the previous layers, generating a segmentation mask.

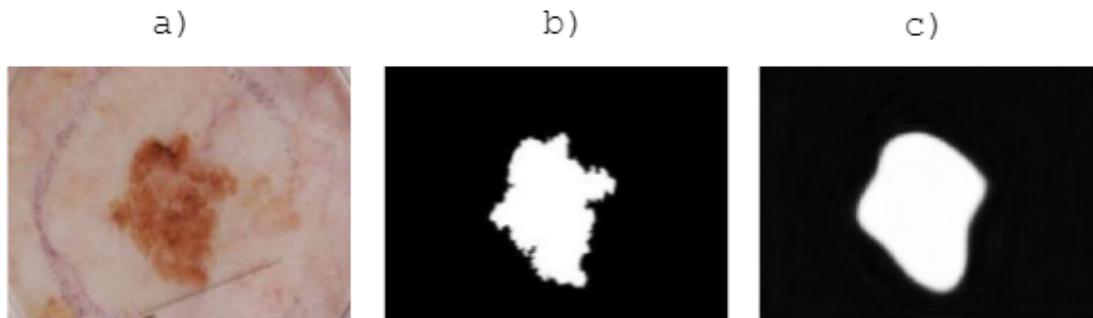


Figure 5.2: Demonstrating the Semantic Pixel-Wise Segmentation (SegNet) results showing the a) original image, b) expert ground-truth and c) SegNet results.

Results in figure 5.2 are generated from the architecture using the ISIC 2018 dataset split into 80% training and 20% validation images. The accuracy of locating the lesions is 85%. However, figure 5.2 represents the border cut-off between skin and skin lesion is accurate to the dataset but inadequate for using the ABCD rules. Finding the border cut-off is vital for measuring ABCD rules [28].

5.2.3 U-Otsu Threshold

Otsu threshold is a versatile automatic image thresholding technique meant to separate each pixel between two classes of foreground or background. One of the benefits of this

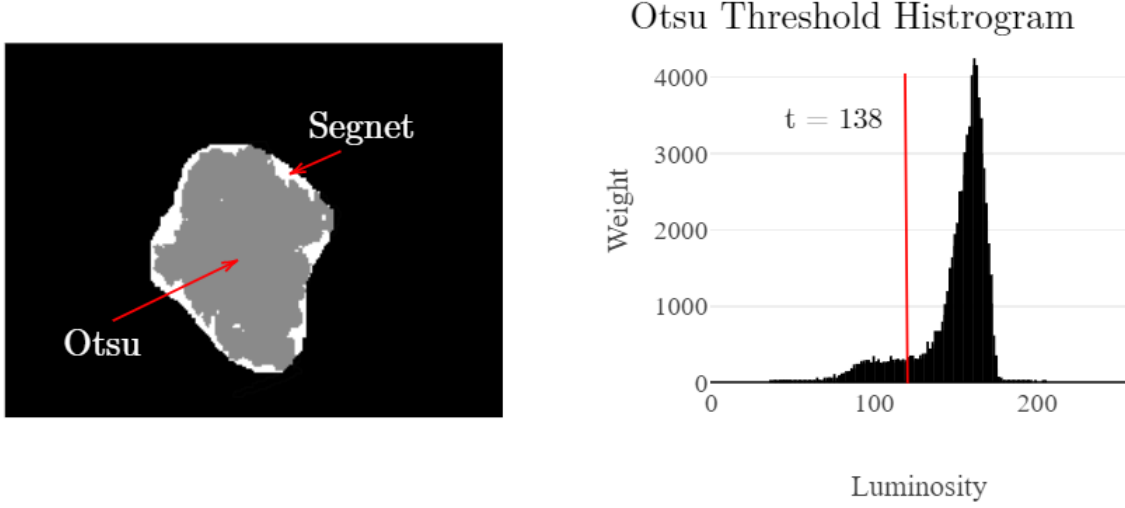


Figure 5.3: Otsu thresholding alongside ground-truth mask, where grey Otsu and white is SegNet. The bar chart shows the histogram with an otsu threshold of 138.

method is that it does not require any training data. The equation 5.2.3 (within-class variance) describes splitting weights of $w_0(t)$, $w_1(t)$, which are the probabilities divided by the threshold t , between 0 and 255. Furthermore, σ_1^2 and σ_0^2 are variances of these two classes. The class probability w is computed from the histogram in figure 5.3, which is an intensity histogram describing the colour distribution in an image. Measuring the values above and below the generated thresholds splits the image into two classes.

$$\sigma_w^2(t) = w_0(t)\sigma_1^2(t) + w_1(t)\sigma_2^2(t) \quad (5.1)$$

The histogram was split into two segments with the threshold t of 138 and the corresponding pixel locations to the histogram segment the skin lesion into two classes. Image morphology closing was applied to fill gaps that the threshold missed. On other occasions, the segmentation missed the skin lesion because of a similar colour between the skin and the skin lesion. It might be beneficial to combine Otsu with SegNet to improve its accuracy while producing a border cut-off. Figure 5.3 describes the difference between otsu and SegNet.

5.2.4 LBPC segmentation

Local Binary Patterns (LBP) is a texture descriptor commonly used for augmenting the image improving classification accuracy[28, 20]. First, equation 5.2 calculates each pixel,

where p (equal to 8) is the number of neighbouring pixels compared to the centre of c , and the radius of r from the centre. Next, shown in equation 5.3 each value is subtracted counter-clockwise with the centre value and compared to function S where each $gp - gc$, if more than or equal to 0, is equal to 1, and less than 0 is equal to 0. Next, add corresponding values equal to 1 of gp together, changing the centre value, ignoring values of 0. Next, applying a Gaussian kernel of 13-pixel iterations and a standard deviation of 3 removes smaller features that interfere with the segmentation. Finally, applying k-means with a value of 2 subtracts the greyscale and segments the skin lesion from the skin.

$$LBP(gp_x, gp_y) = \sum_{p=0}^{P-1} s(gp - gc)2^p \quad (5.2)$$

$$s(x) = \begin{cases} 1, & x \geq 0; \\ 0, & \text{otherwise.} \end{cases} \quad (5.3)$$

Figure 5.2.4 demonstrates the segmentation of two skin lesions, one with an irregular border and another with a regular border. LBPC is applied to both skin lesions, followed by Gaussian blurring and morphology closing to remove dots. The result is an improved border cut-off compared to the ground truth in the Ph² dataset with more corners and ledges. This technique will improve accuracy for measuring border irregularity[28].

Validating LBPC is not expected because the goal is to exaggerate the border to improve the classification process of ABCD rules, which it does successfully[28, 20]. For example, the segmentation might not match dataset segmentations but is still essential to classifying ABCD rules. Furthermore, many datasets lack expert border segmentation, an accurate border cut-off between the skin and skin lesions, so comparisons are not always possible.

5.2.5 Results

Overall the accuracy of the techniques demonstrates that SegNet is the most reliable technique. However, comparing the techniques in ?? we can demonstrate that it produces a smudge effect and fails to capture the border cut-off from the skin lesion, but it is successful at finding the location of the skin lesion.

Both statistical models of LBPC and Otsu threshold generated an accurate border cut-off between the skin and the skin lesion As previously mentioned, measuring the border cut-off and exaggerating irregular borders are helpful when calculating the ABCD rules.

It might be beneficial to combine SegNet and LBPC using SegNet to find the skin lesions' location, followed by adjusting the border cut-off using LBPC. A similar technique using the Otsu threshold and Segnet is described by[30].

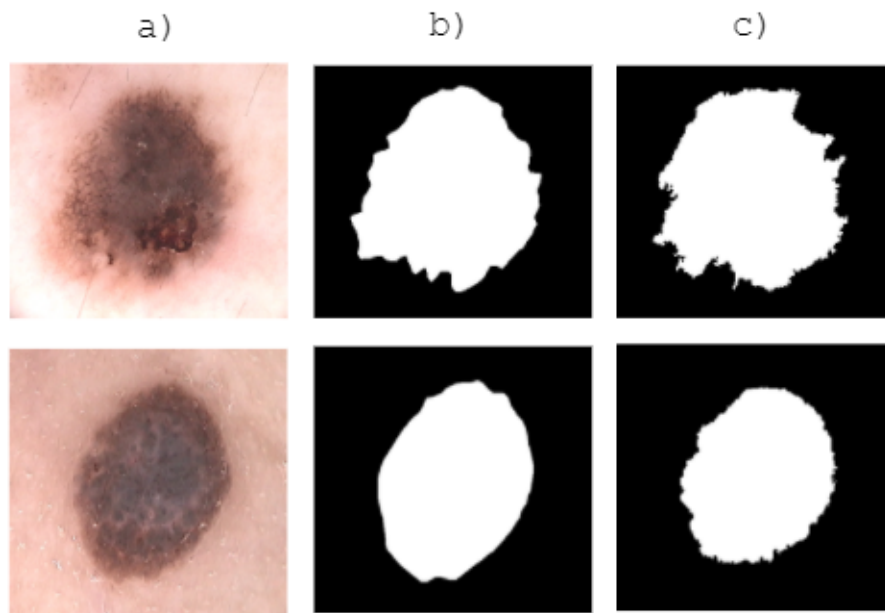


Figure 5.4: Local Binary Pattern Clustering (LBPC) showing the a) original image, b) ground-truth, and c) LBPC. LBPC successfully exaggerates the border cut-off on the skin lesions with regular and irregular borders

5.2.6 Results of Border Cut-off

This section includes a simple border analysis technique called fractal box counting to assess the benefits of using different segmentation algorithms with accurate border cut-offs.

To prove the usefulness of segmentation techniques with an accurate border cut-off a technique developed by Ali[4] is implemented that utilises machine learning with extracted data including Zernike moments, fractal box-counting, and convexity measurements. Fractal box-counting is used to measure the irregularity of the border.

The fractal box-counting technique is a commonly employed technique for analysing fractal properties. It involves dividing a fractal object or pattern into a grid of equally sized boxes and counting the number of boxes that contain a portion of the fractals. The process is repeated with different box sizes until the relationship between the box sizes and number of boxes is analysed determining the fractal dimension[Hamburger1996]. Essentially a more complicated border with corners and convexes will have more boxes and therefore a higher fractal score, than for example a border with smooth corners and edges which has a lower score. This should provide some evidence of the usefulness of an accurate border.

5.3 Issues

The segmentation algorithms encountered some issues, whilst the best of the techniques was SegNet with an 85% accuracy when relating to the ISIC 2019 dataset. However, as previously mentioned the segmentation masks have poor border cut-off stunting features that are useful for finding border irregularities.

In contrast LBPC and U-Otsu algorithms effectively identify the border cut-off of the skin lesion, which isn't properly represented in the ISIC 2019 dataset. But, it sometimes fails to find the skin lesion or not detect anything.

Both techniques appear to have downfalls making them less effective for use for analysing ABCD rules. It would be beneficial to find the approximate area of the skin lesion using SegNet and followed by LBPC to find the border cut-off.

5.3.1 Joint Neural network and statistical model approach

Combining both SegNet and LBPC improves the accuracy.

5.4 ABCD Rules Data Extraction Techniques

Melanoma is a type of malignant skin cancer that accounts for a significant proportion of cancer-related deaths around the world. In 2018 there were approximately 2,353 per 100,000 deaths in the United Kingdom (UK)[44]. Early detection is critical for improving

the diagnosis and survival of patients. However, existing approaches including clinical examinations and dermoscopy, have limitations in terms of accuracy and cost-effectiveness[39]. Machine learning approaches have beaten dermatologists in terms of accuracy[7]. However, these approaches lack explainability implementing such techniques difficult for clinical environments[15]. One concern is the production of realistic, but incorrect results[17]. Another is the use of parallel processes, which describes the creation of an answer with little to no explanation. In this paper, we propose a combined asymmetry approach using shape, colour, and texture analysis alongside a detailed comparison. The technique itself can be used in conjunction with ABCD rules (Asymmetry, border, colour, and dermoscopic features).

5.4.1 Preferred Diagnostic Procedures

Diagnostic procedures are procedures that are performed on patients in order to diagnose conditions. Regarding the diagnosis of melanoma, many types have been utilised for the detection of melanoma and the most favourable are CASH, ABCD rules, and Total Dermoscopy Score (TDS). The ABCD rules and TDS were commonly used because of their simplicity and effectiveness.

Diagnostic procedures are usually based on the doctors medical experience. For example the use-case of this project is for general practioners (GPs), many of which have likely never seen or attempted to diagnose melanoma, and many of which will not have access to dermoscopes for the analysis of dermoscopic structures. So, in this use-case diagnostic procedures including ABCD rules, and CASH are suitable because of their simplicity. The method used by the NHS is also ABCD rules, which is the reasoning for using this method.

Interestingly dermatologists will utilise dermoscopic features and textures, which are more accurate but require sufficient training for the detection.

Asymmetry Techniques

Asymmetry analysis is a fundamental component in the early detection of melanoma because it often exhibits asymmetric shapes[3]. Meaning that the shape, colour and, texture match asymmetrically more often in benign lesions. For example, as melanoma grows the central area begins to waste away leaving a hollow area covered by thin skin, showing dermoscopic features. As it grows the edges become more irregular producing an uneven shape often relating to irregular borders and asymmetrical shapes. Diagnostic procedures have been developed to detect these unique characteristics.

Bi-fold is a diagnostic procedure designed to support the recognition of melanoma by drawing a line down the middle of the skin lesion and comparing the two halves to confirm whether the sides match (considering the difference in shape, colour, and texture). Using this horizontally and vertically calculates whether the skin lesion is possibly malignant with a score between 0 and 2. Calculating with Total Dermoscopy Score (TDS) alongside

the other ABCD rules including asymmetry, border, colour, and diameter calculates the likelihood of malignancy. Dermatologists frequently use bi-fold due to its simplicity, but it can be subjective to the original observer and time-consuming when managing large numbers of skin lesions. Therefore, automating techniques is beneficial to clinicians and can improve the objectivity of results.

5.4.2 Related Works

Ihab S. Zaqout[48] describes a technique using the centroid and rotation of the skin lesion using moments of inertia. By Folding the skin lesion on both vertical and horizontal axes subtracting the opposite half. Pixels that cannot subtract are summed and compared with a threshold considering the skin lesion asymmetrical if the combined sum is more than the threshold.

Kasmi and Mokrani[19] create a grid of 20 by 20 pixels from the skin lesion image and convert it into the LAB colour space. They then compare the average colour of each block with a perpendicular block (vertical and horizontal axes) using the three-dimensional Euclidean luminance distance, a-axis, and b-axis. If more than half of the colour comparisons exceed the threshold, they consider that axis to be colour asymmetrical. They ignore blocks that have no symmetrical pair. Finally, they calculate luminance separately to prevent brightness problems. This technique achieves an accuracy of 94% with a private dataset.

Ali[3] uses SIFT-based similarity and projection profiles to measure similarities in texture. SIFT is scale-invariant and helpful for texture components with varying texture quality. First, they split the skin lesion vertically and horizontally across the centre into four halves, compare texture components on the symmetrical halves, and measure similarity. Lastly, they generate histograms for the projection profile in the x and y directions. These results train a decision tree and achieve an 80% accuracy of the ISIC 2018 with 204 images privately annotated for ABCD rules.

Prior studies have introduced techniques that measure distinct aspects of asymmetry, such as Ihab S. Zaqout[48] measurement of shape, Kasmi and Mokrani[19] measurement of colour, and Ali[3] measurement of texture. The new approach seeks to combine the following approaches into a more comprehensive analysis of asymmetry that takes into account multiple features of the skin lesion. The proposed novel technique updates colour measurement to improve accuracy using superpixels and an SVM model.

5.5 A Novel Asymmetry detection technique using Bi-Fold, 3D Euclidean distance, and Superpixels

This section describes a novel machine-learning technique for the automatic detection of melanoma

5.5.1 Bi-fold

To initiate the classification of skin lesions a technique called bi-fold is applied involving folding the skin lesion in half vertically and horizontally and a comparison of their respective dimensions. While the original technique was designed only to assess the lesions' shape, it's been utilized to account for colour and texture as well. The centre and orientation are determined by calculating its moments, where the centre is $(m_{10} / m_{00}, m_{01} / m_{00})$ and ϕ is $0.5 \tan (2m_{11}) / (m_{20} - m_{02})$.

5.5.2 3D Euclidean Distance

Next, the lesion is partitioned into a 20 by 20 grid centred on the mentioned centre point, and the average of each region is computed. This is followed by finding the matching region on the perpendicular area from the centre of the skin lesion and comparing the colour distance between the two. Distance is measured using the LAB colour space and a 2D Euclidean distance of A and B, removing L (luminosity) to eliminate light variation. Once compared, all compared regions are obtained, and they are plotted onto a graph. If over half of the values are above a threshold of 6, then the lesion is asymmetrical.

The diagram shown below in figure 5.5.2 is a compilation of all the images within the PH2 dataset showing the threshold range after applying bi-fold, euclidean distance of colour, but before applying the threshold. As can be seen, a threshold of 6 covers all of the symmetrical values, but still roughly covers half of the asymmetrical values. This demonstrates that the technique produces many false positives when regarding asymmetrical values. Essentially, the symmetrical skin lesion has a smaller area and the asymmetrical lesion has a larger area, but both remain in the same zone and therefore splitting the data only using a threshold holds poor results. Furthermore, there are a lot of fliers and the threshold does not adjust according to these values. See the graph below:

To improve the accuracy of the algorithm some changes need to be made based on the previous statements. First will be superpixels and next is k-means.

5.5.3 Superpixels using Simple Linear Iterative Clustering (SLIC)

Superpixel is an algorithm for grouping pixels into a grid format, but with flexible borders that can adjust to regions with similar features. Unlike the original technique averaging specific squares in a grid [19], they are segmented related to colour, texture, and other properties. The reason for using this technique is to increase boundary adherence and to group features that might otherwise be split into separate groups. This overall improves the accuracy of the algorithm.

This technique uses a simple linear iterative clustering (SLIC) algorithm and was first introduced by Achanta et al. [1]. This technique combines both k-means and graph-based segmentation. Firstly you define the desired number of superpixels as k and the approximate size of each superpixel as S , which is usually $S = \sqrt{\text{square}(N/k)}$ and N is the number of

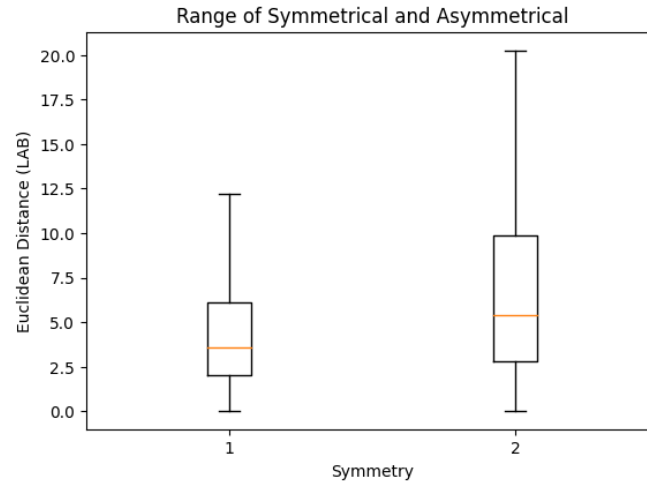


Figure 5.5: This diagram is a summary of the PH2 dataset after using bi-fold, a euclidean distance of colour. The value on the right would be a threshold.

pixels in the image. Secondly, for the centre of each cluster, a search space is assigned to the cluster. For each group, you measure the spatial distance which is the Euclidean distance between each pixel and the cluster center. Each pixel is assigned to the cluster with the nearest centroid. The cluster centres are then recalculated by taking the mean colour and position of the pixels assigned to each cluster. Followed by new pixels being assigned to the centroid relating to Euclidean distance. This process is repeated depending on the number of iterations as i are assigned. From this point, each pixel is assigned to a cluster.

The image in ... demonstrates the usual average and the new averages based on superpixels and the changes in values. Areas that are lighter in colour appear to have a lower value and darker appear darker.

Using the thresholding method for classification we can already see the accuracy has been improved with a threshold of ...

5.6 Experimental Results

The goal of this experiment is to improve the accuracy of the asymmetry bi-fold technique described by Ihab S. Zaquout et al.[48]. Initially, the skin lesion is split into a 10 by 10 grid and converted into the LAB colourspace. Next, a line is drawn through the middle horizontally and vertically. Measuring the Euclidean distance from the centroid, locating the closest opposite patch of colour finds the parallel square. Subtracting the squares generates a score for each value, the closer to 0, the more similar the colour. These are then removed from the list to prevent them from being selected a second time. If half the results are over a

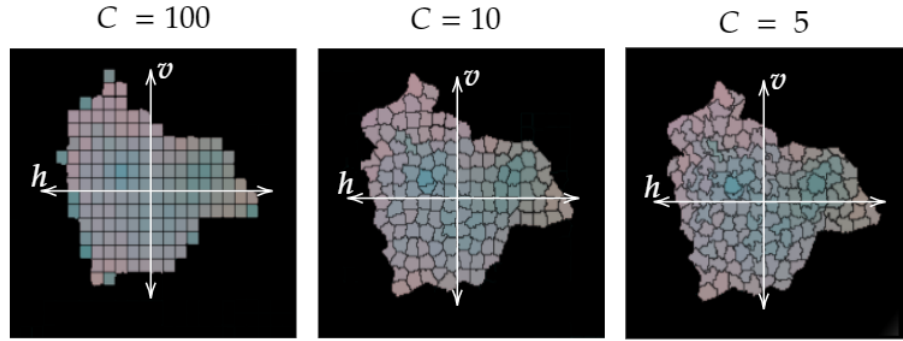


Figure 5.6: This diagram shows the skin lesion split relating to superpixels instead of averaging squares.

specific threshold, it is considered asymmetrical in colour, otherwise considered symmetrical. The aim is to make a 10 by 10 grid, but instead of averaging squares, superpixels reduce data redundancy in the grid, allowing for a less complex algorithm and improving accuracy. The clustering method k-means partitions each pixel to its nearest most similar centroid relating to colour. Next, it generates a superpixel that represents the average colour of that area. The diagram 5.6 demonstrates different borders when changing the C for compactness, where 100 generates a square grid similar to the original technique. The border becomes more flexible as the compactness value decreases.

Each parallel square on the vertical and horizontal axes measures similarity using a three-dimensional Euclidean distance in the LAB colour space. For example, the perceivable difference of colour to the human eye is a three-dimensional Euclidean distance of 6[26]. Using similar logic, a value of 20 is the threshold, where any value over that amount is considered asymmetrical in colour. Next, each square is compared with its closest parallel square (relating to the line through the centre defined by the bi-fold) and removed from an array after being compared. The next improvement is to generate a unique threshold for the significance of each square. For example, using superpixels with the compactness of 10 has an accuracy of 61% with the PH² dataset compared to the original 59.5%. This approach demonstrates that a flexible border that considers features is more effective than averaging squares.

There is a correlation in colour differences between the inner and outer edges because melanoma typically expands outwards, creating an abnormal border. This information specifies that the statistical model accuracy could be improved by increasing the threshold for the outer edges and decreasing it for the inner.

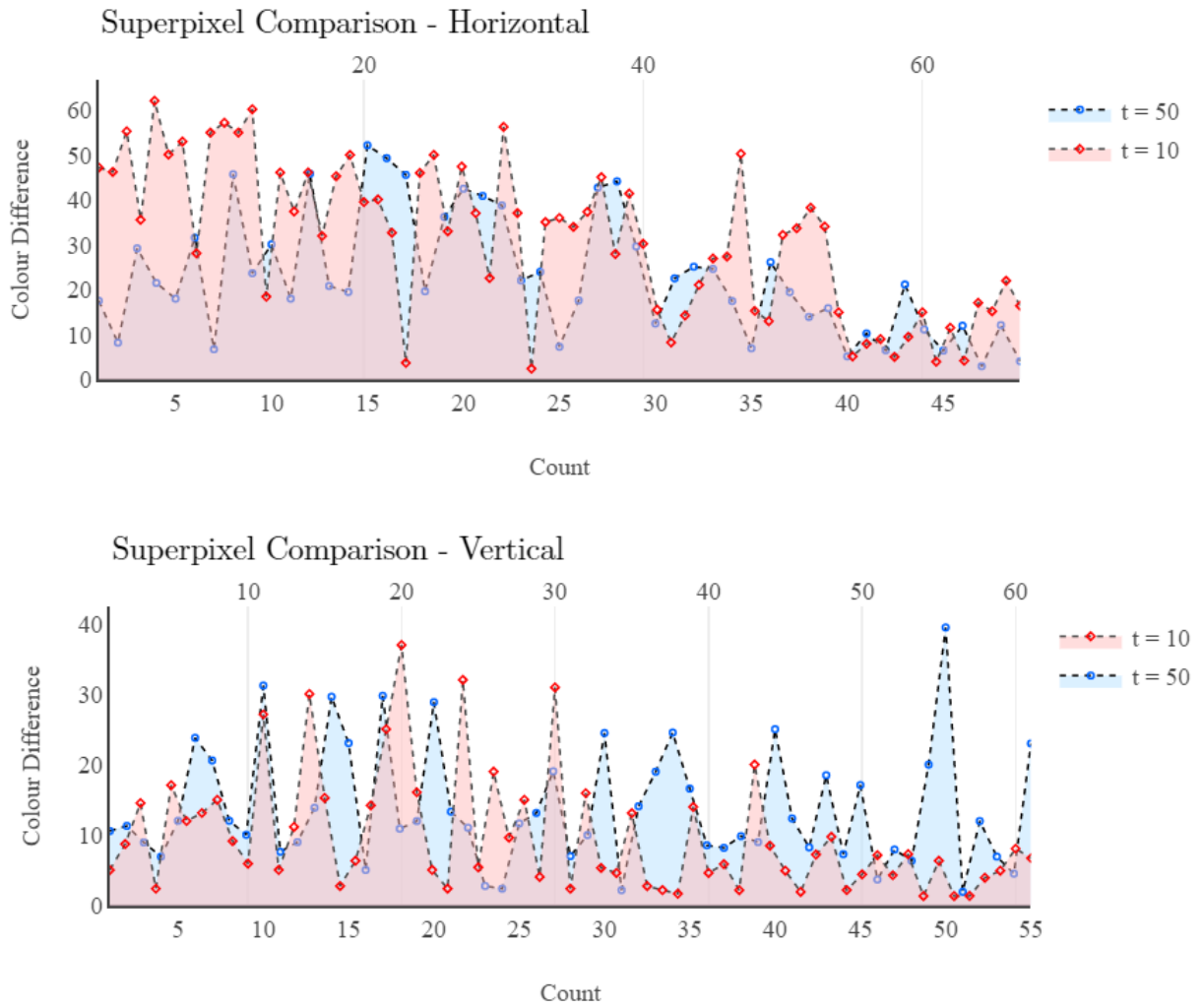


Figure 5.7: This diagram shows the difference between averaging squares and using superpixels, with the threshold of 10 implying curves and 50 being squares. The horizontal colour difference is improved, making it more likely to be seen asymmetrical. The vertical comparison is roughly the same, except for removing a false positive of 40.

5.7 Border Detection Using Zernike Moments, Fractal Box-Counting, and Convexity

5.8 A Novel Colour Analysis Approach using Colour Ranges, and SVM

5.9 Dermoscopic structures

5.10 Results

5.11 Conclusion

Chapter 6

Case-Based Reasoning (CBR)

Chapter 7

Combined ABCD Rules and Dermoscopic Structures using Bayesian Network

7.1 Introduction

In this chapter, we focus on the creation of a novel CAD framework that aims to automate the ABCD rules (Asymmetry, Border, Colour, and Dermoscopic structures) using SVM models and Bayesian fusion. To incorporate case-based reasoning, an Artificial Neural Network (ANN) is implemented to identify skin lesions with similar features.

This chapter proposes a CAD framework for the detection of melanoma using data extraction techniques to ensure the use of relevant features. The aim is to produce a transparent system focusing on providing information that would be useful to dermatologists and the impact of those features on the diagnosis. Metadata is included regarding age, gender, and anatomical location. Other features are asymmetry, border, colour, and dermoscopic structures. These are then combined using a Bayesian network. Case-based reasoning is also implemented to find skin lesions with similar clinical features.

7.2 Background

Automatic systems are being developed for the early detection of melanoma because it can take 10 years of experience for an accuracy of 86%[25]. Melanoma is one of the most aggressive forms of cancer that can remain dormant from anywhere between 6 months and 10 years before developing into metastatic melanoma, which becomes substantially more difficult to cure[44]. Problematically, clinicians who are not trained specifically to diagnose melanoma are usually the first to attempt it. Improving the accuracy of these clinicians should increase the overall accuracy of detecting melanoma. The early detection of melanoma followed by

a biopsy is known to completely cure the disease[mohammadpour2019]. Furthermore, melanoma develops from melanocytes that create skin pigmentation through the production of melanin, making a brown patch on the skin. Therefore, it has a clear indication of development on the surface of the skin. This means it is ideal for the creation of computer vision models for early detection.

For these reasons, there has been further interest in developing an automatic system for helping clinicians detect melanoma at its early stages. However, regardless of newer systems being developed they are still rarely implemented within clinical environments. This is largely due to systems producing parallel diagnosis, which does not explain how results were reached[21, 7]. These techniques usually utilise Convolutional Neural Networks (CNN) because of their superior accuracy[Wen2022]. There should be further explanations of the diagnosis for clinicians to understand and properly utilise within clinical environments.

Newer machine learning models utilise explainable AI (XAI) to provide an explanation that provides further insight[skar2017]. While these provide some indication of which area of the image has been used to train the algorithm they are still not tied directly to relevant clinical features. Furthermore, there appears to be a tradeoff between interpretability and model performance. Clinicians might not want to utilise models that are more interpretable, but less accurate. Furthermore, there has been some indication of models producing realistic but incorrect results[21]. In some scenarios, clinicians might be misled to falsely diagnose a skin lesion. Due to the high stakes involved when diagnosing melanoma, there should be highly accurate explanations and a track record of success before utilising them.

7.3 Related Work

In the design of CAD systems, two types of algorithms are employed. The initial type involves feature extraction, which is followed by individual classification methods. This process holds significant importance as it ensures the utilisation and visualisation of clinical features. The latter algorithm utilises the extracted features to classify different types of skin lesions. This method produces clinically relevant features that facilitate the diagnosis.

7.3.1 Feature Extraction algorithms

Ihab S. zaqout[48] describes a technique using the centroid and rotation of the skin lesion using moments of inertia. The skin lesion is folded over vertically and horizontally subtracting the opposite halves. Pixels that cannot be subtracted are summed and compared with a threshold. If over the threshold the skin lesion is considered asymmetrical in that direction.

Reda Kasmi and Karim Mokrani[19] describe a technique for comparing the colour distribution of the skin lesion by splitting the lesion into a 20 by 20 grid and comparing it against the colour of the perpendicular square using the 3D Euclidean distance. If over a

threshold that square is considered asymmetrical. If more than half the lesions are over the threshold then the area is considered asymmetrical.

7.3.2 Classification Methods

A paper described by Javier Lopez, et al.[22] describes a CAD system designed to provide clinicians with an enriched diagnosis. They utilise data extraction and classification techniques on dermoscopic structures, followed by combining the output of individual features using a Bayesian approach. This provides an indication of which features impact the diagnosis.

7.4 Proposed Method

The proposed CAD framework described in Figure 7.1 automates the ABCD rules using statistical algorithms to extract features (f) from asymmetry, border, colour, and dermoscopic structures. Each feature has an associated SVM model trained using these extracted features. Next, Bayesian fusion, a probabilistic approach, combines multiple independent classifiers to diagnose melanoma. One benefit of Bayesian fusion is its higher accuracy in classifying skin lesions as compared to a standalone classifier[40]. Javier López-Labraca, et al describe a similar method using dermoscopic structures, and colour[22]. Other benefits are estimating the relevance of individual classifiers and classifying them with incomplete data, making it an interpretable and robust method. In addition, some feature extraction techniques generate graphics that might be suitable as an explanation for the diagnosis. Finally, the PH² dataset validates the rules, and once combined into a diagnosis, more extensive datasets, including ISIC 2019, measure its accuracy based on the diagnosis.

The ABCD rules, a set of criteria employed for the early detection of skin cancer, especially melanoma, are instrumental in guiding clinicians and individuals in assessing potentially suspicious skin lesions. The acronym "ABCD" stands for asymmetry, border irregularity, color variation, and diameter. Each element serves as a crucial parameter in evaluating the characteristics of moles or lesions on the skin. The objective of utilising this diagnostic procedure is to visualise important features that GPs need to support their diagnosis. Automating this process will instantiate trust when automating skin lesion identification within clinical environments. Another advantage would be the automatic labelling of skin lesions, making it easier for dermatologists to identify later.

The CAD framework in figure 7.1 describes a model of pre-processing, feature extraction, and classification stages. After segmentation, statistical algorithms extract features (f), representing a different rule. Next, SVM models individually process the extracted features and combine them into a final result between benign and malignant using Bayesian fusion.

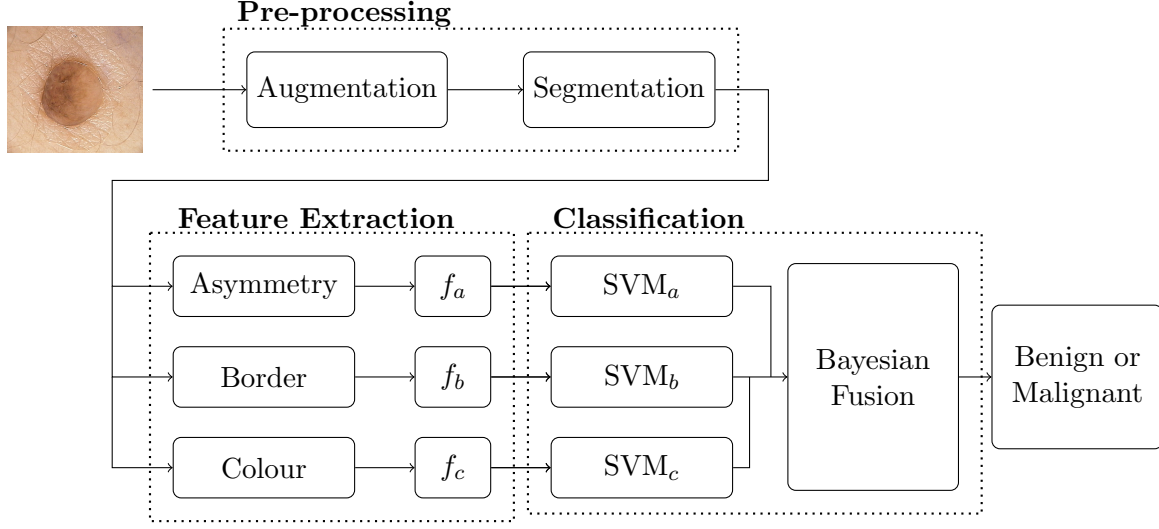


Figure 7.1: Proposed CAD framework describing the segmentation, feature extraction and classification process.

7.4.1 Feature Extraction Methods

ABCD rules in this refer to the asymmetry, border irregularity, colour variation, and dermoscopic structures. Sometimes the D in ABCD rules refers to the diameter of the skin lesion, but it is often removed for dermoscopic structures because images are taken at different distances making the measurement of diameter unreliable. Furthermore, the detection of dermoscopic structures provides valuable information in detecting the melanoma mimic called seborrhoeic keratosis (SK)[24].

Asymmetry

The approach for identifying asymmetry in this chapter is adapted from the work of Reda Kasmi and Karim Mokrani[19]. In the original method, a bi-fold technique is employed to determine the centroid and rotation of the skin lesion, followed by image rotation. Subsequently, the image undergoes a conversion to LAB colorspace and is divided into a 20 by 20 grid by averaging color areas. The modified technique, however, utilizes superpixels from Simple Linear Iterative Clustering (SLIC) introduced by Achanta et al.[1], with a compactness (C) set to 20.

Each color square is compared with others perpendicular to the centroid (with bi-fold) using the 3D Euclidean distance of the color (LAB). The resulting distance score is accumulated in an array, and if more than half exceed a threshold of 6, the lesion is classified as asymmetrical, contributing a TDS score of 1. This process is repeated at a 90-degree orientation, adding another TDS score if asymmetry is detected.

The data presented in Figure?? illustrates that employing superpixels better supports the thresholding process compared to the original technique. The boxplot data represents the Euclidean distance, summed and divided by the number of positions.

Colour

Dermoscopic Structures

7.4.2 Bayesian Fusion using Naive Bayes

Bayesian fusion is a class of methods used to combine information from multiple sources taking into account uncertainty and probability distributions. This technique is frequently used for medical diagnosis for integrating data from various diagnostic tests to improve the accuracy of disease diagnosis[empty citation].

7.4.3 Case-Based reasoning using Artificial Neural Network (ANN)

7.5 Results

Two datasets were utilised to test the produced algorithms. The first is the PH2 dataset which includes asymmetry, colour, and dermoscopic structures.

7.6 Discussion

7.7 Conclusion

Chapter 8

Conclusion

Validating the automatic ABCD rules is challenging because public datasets are scarce and often lack sufficient data. For example, PH² contains 200 images on asymmetry, colour, and some dermoscopic structures but misses border irregularity. Therefore researchers aiming to measure borders use private or privately annotated datasets. Furthermore, many papers measuring asymmetry, colour and dermoscopic structures lack validation using public datasets despite PH² being available at the date of their publication. On the other hand, public datasets are crucial to comparing, validating, and reproducing algorithms. Therefore ABCD rules (apart from the border) will be validated using PH² datasets so that future researchers can replicate techniques. Furthermore, once rules are combined using Bayesian fusion, a type of probabilistic analysis, results can conform to the diagnosis between malignant and benign, validated from larger datasets, including ISIC 2019.

Finding the border cut-off is fundamental for the classification of melanoma using the ABCD rules[28]. Many valuable techniques use statistical models, including LBPC and Otsu, instead of transposed CNNs such as SegNet. Hybrid approaches using SegNet followed by Otsu to measure the border cut-off have been proven beneficial. However, using SegNet without a statistical model is worse when used with the ABCD rules than current methods such as LBPC and Otsu. Therefore, exploring other statistical segmentation techniques and hybrids would be beneficial. Furthermore, segmentation ground-truths do not always correspond to good classification accuracy with ABCD rules, which means even a low accuracy segmentation compared to datasets might have better accuracy when classifying the ABCD rules for border irregularity.

Statistical models for asymmetry, border, and colour extract relevant features for melanoma classification. The goal is to mimic the diagnostic procedure that clinicians are familiar with to produce results that they can utilise in a clinical environment. Extracting relevant features using box-counting and bi-folds ensures capturing relevant features and that the technique is retractable. However, accuracy is lacking in these techniques where superpixels improved asymmetry, changing the accuracy from 58.5% to 61% for the PH²

dataset. Further improvements will be made after training an SVM model using the extracted features. Further implementation of convexity and Zernike moments for border irregularity will improve the accuracy. Furthermore, implementing a texture comparison for asymmetry measurements improve accuracy again.

Chapter 9

Future Work

Developing algorithms to extract features of ABCD rules is beneficial to GPs because it improves interpretability. Future work will involve extracting more features and training SVM models. For example, extracting more relevant asymmetry features will help classify asymmetry as there is currently no unification of shape, colour, and texture into a single classification model. The extracted features will be combined into a diagnosis between benign and malignant using a Bayesian probabilistic network. Bayesian probability is beneficial because its highly accurate[40] and modifiable and ability to classify with incomplete data. For example, asymmetry, border, and colour are sometimes enough to classify skin lesions. However, in some cases, dermoscopic structures or other meta-data, including age, gender, touch, feeling, and location on the body, are required for an accurate diagnosis. Furthermore, This might benefit GPs because it encourages considering a wide range of not always considered features.

Melanoma evolves from benign lesions at initially 30%-50%, and despite its significance, clinicians or computers are not yet able to reliably predict this change. AI trained on relevant images could predict melanoma before it occurs[36]. Data on skin lesion evolution is rare in public datasets. However, the associated organisation has taken images of the same skin lesion multiple times. It would be incredibly beneficial to assess the quality of these images, which could potentially lead to the development of a technique describing evolution. Considering evolution in machine learning techniques in the future would be incredibly beneficial to the early detection of melanoma but can only be achieved when there is more data.

Bibliography

- [1] Radhakrishna Achanta et al. “SLIC superpixels compared to state-of-the-art superpixel methods”. In: *IEEE Transactions on Pattern Analysis and Machine Intelligence* 34 (11 2012). ISSN: 01628828. DOI: 10.1109/TPAMI.2012.120.
- [2] Saleh Albahli et al. “Melanoma Lesion Detection and Segmentation Using YOLOv4-DarkNet and Active Contour”. In: *IEEE Access* 8 (2020). ISSN: 21693536. DOI: 10.1109/ACCESS.2020.3035345.
- [3] Abder Rahman Ali, Jingpeng Li, and Sally Jane O’Shea. “Towards the automatic detection of skin lesion shape asymmetry, color variegation and diameter in dermoscopic images”. In: *PLoS ONE* 15 (6 2020). ISSN: 19326203. DOI: 10.1371/journal.pone.0234352.
- [4] Abder-Rahman Ali et al. “A machine learning approach to automatic detection of irregularity in skin lesion border using dermoscopic images”. In: *PeerJ Computer Science* 6 (2020), e268. ISSN: 2376-5992. DOI: 10.7717/peerj.cs.268/table-3.
- [5] Abder Rahman H. Ali, Jingpeng Li, and Guang Yang. “Automating the ABCD Rule for Melanoma Detection: A Survey”. In: *IEEE Access* 8 (2020), pp. 83333–83346. ISSN: 21693536. DOI: 10.1109/ACCESS.2020.2991034.
- [6] Murali Anantha, Randy H. Moss, and William V. Stoecker. “Detection of pigment network in dermatoscopy images using texture analysis”. In: *Computerized Medical Imaging and Graphics* 28 (5 2004). ISSN: 08956111. DOI: 10.1016/j.compmedimag.2004.04.002.
- [7] Esteva Andre et al. “Dermatologist-level classification of skin cancer with deep neural networks”. In: *Nature* 542 (7639 2017), pp. 115–118. ISSN: 1476-4687. DOI: 10.1038/nature21056LK-http://elinks.library.upenn.edu/sfx_local?sid=EMBASE&issn=14764687&id=doi:10.1038%2Fnature21056&atitle=Dermatologist-level+classification+of+skin+cancer+with+deep+neural+networks&stitle=Nature&title=Nature&volume=542&issue=7639&spage=115&epage=118&aualast=Esteva&aufirst=Andre&aunit=A.&aufull=Esteva+A.&coden=NATUA&isbn=&pages=115-118&date=2017&aunit1=A&aunitm=. URL: <http://www.embase>.

- com/search/results?subaction=viewrecord&from=export&id=L614981551%0Ahttp://dx.doi.org/10.1038/nature21056.
- [8] Alejandro Barredo Arrieta et al. “Explainable Explainable Artificial Intelligence (XAI): Concepts, taxonomies, opportunities and challenges toward responsible AI”. In: *Information Fusion* 58 (2020), pp. 82–115. ISSN: 15662535. DOI: 10.1016/j.inffus.2019.12.012.
 - [9] Vijay Badrinarayanan, Alex Kendall, and Roberto Cipolla. “SegNet: A Deep Convolutional Encoder-Decoder Architecture for Image Segmentation”. In: *IEEE Transactions on Pattern Analysis and Machine Intelligence* 39 (12 2017), pp. 2481–2495. ISSN: 01628828. DOI: 10.1109/TPAMI.2016.2644615.
 - [10] Shailender Bhatia, Scott S. Tykodi, and John A. Thompson. *Treatment of metastatic melanoma: An overview*. 2009.
 - [11] Liang Chieh Chen et al. “DeepLab: Semantic Image Segmentation with Deep Convolutional Nets, Atrous Convolution, and Fully Connected CRFs”. In: *IEEE Transactions on Pattern Analysis and Machine Intelligence* 40 (4 2018). ISSN: 01628828. DOI: 10.1109/TPAMI.2017.2699184.
 - [12] Armand B. Cognetta et al. “The ABCD rule of dermatoscopy: High prospective value in the diagnosis of doubtful melanocytic skin lesions”. In: *Journal of the American Academy of Dermatology* 30 (4 1994), pp. 551–559. ISSN: 01909622. DOI: 10.1016/S0190-9622(94)70061-3.
 - [13] A. Dascalu et al. “Non-melanoma skin cancer diagnosis: a comparison between dermoscopic and smartphone images by unified visual and sonification deep learning algorithms”. In: *Journal of Cancer Research and Clinical Oncology* 148 (9 2022). ISSN: 14321335. DOI: 10.1007/s00432-021-03809-x.
 - [14] Vincent Dick et al. “Accuracy of Computer-Aided Diagnosis of Melanoma: A Meta-analysis”. In: *JAMA Dermatology* 155 (11 2019), pp. 1291–1299. ISSN: 21686068. DOI: 10.1001/jamadermatol.2019.1375.
 - [15] Haidi Fan et al. “Automatic segmentation of dermoscopy images using saliency combined with Otsu threshold”. In: *Computers in Biology and Medicine* 85 (2017), pp. 75–85. ISSN: 18790534. DOI: 10.1016/j.compbiomed.2017.03.025.
 - [16] Masaru Fuji et al. “Explainable AI through combination of deep tensor and knowledge graph”. In: *Fujitsu Scientific and Technical Journal* 55 (2 2019), pp. 58–64. ISSN: 00162523.
 - [17] Amirata Ghorbani, Abubakar Abid, and James Zou. “Interpretation of Neural Networks Is Fragile”. In: *Proceedings of the AAAI Conference on Artificial Intelligence* 33 (2019), pp. 3681–3688. ISSN: 2159-5399. DOI: 10.1609/aaai.v33i01.33013681.

- [18] Leonid Izikson et al. “Prevalence of melanoma clinically resembling seborrheic keratosis: Analysis of 9204 cases”. In: *Archives of Dermatology* 138 (12 2002). ISSN: 0003987X. DOI: 10.1001/archderm.138.12.1562.
- [19] Reda Kasmi and Karim Mokrani. “Classification of malignant melanoma and benign skin lesions: Implementation of automatic ABCD rule”. In: *IET Image Processing* 10 (6 2016), pp. 448–455. ISSN: 17519659. DOI: 10.1049/iet-ipr.2015.0385.
- [20] Sertan Kaya et al. “Abrupt skin lesion border cutoff measurement for malignancy detection in dermoscopy images”. In: *BMC Bioinformatics* 17 (2016). ISSN: 14712105. DOI: 10.1186/s12859-016-1221-4.
- [21] Zachary C. Lipton. “The mythos of model interpretability”. In: *Communications of the ACM* 61 (10 2018). ISSN: 15577317. DOI: 10.1145/3233231.
- [22] Javier López-Labraca et al. “Enriched dermoscopic-structure-based cad system for melanoma diagnosis”. In: *Multimedia Tools and Applications* 77 (10 2018), pp. 12171–12202. ISSN: 15737721. DOI: 10.1007/s11042-017-4879-3.
- [23] E. Meskini et al. “A new algorithm for skin lesion border detection in dermoscopy images”. In: *Journal of Biomedical Physics and Engineering* 8 (1 2018), pp. 109–118. ISSN: 22517200. DOI: 10.22086/jbpe.v0i0.444.
- [24] Akane Minagawa. “Dermoscopy–pathology relationship in seborrheic keratosis”. In: *Journal of Dermatology* 44 (5 2017), pp. 518–524. ISSN: 13468138. DOI: 10.1111/1346-8138.13657.
- [25] C. A. Morton and R. M. Mackie. “Clinical accuracy of the diagnosis of cutaneous malignant melanoma”. In: *British Journal of Dermatology* 138 (2 1998). ISSN: 00070963. DOI: 10.1046/j.1365-2133.1998.02075.x.
- [26] Nikolaos E. Myridis. “Ultra-realistic Imaging: Advanced Techniques in Analogue and Digital Colour Holography, by Hans Bjelkhagen and David Brotherton-Ratcliffe”. In: *Contemporary Physics* 55 (3 2014), pp. 247–248. ISSN: 0010-7514. DOI: 10.1080/00107514.2014.907348.
- [27] Franz Nachbar et al. “The ABCD rule of dermatoscopy”. In: *Journal of the American Academy of Dermatology* 30 (4 Apr. 1994), pp. 551–559. ISSN: 01909622. DOI: 10.1016/s0190-9622(94)70061-3.
- [28] Pedro M.M. Pereira et al. “Skin lesion classification enhancement using border-line features – The melanoma vs nevus problem”. In: *Biomedical Signal Processing and Control* 57 (2020). ISSN: 17468108. DOI: 10.1016/j.bspc.2019.101765.
- [29] Maryam Ramezani, Alireza Karimian, and Payman Moallem. “Automatic Detection of Malignant Melanoma using Macroscopic Images”. In: *Journal of Medical Signals and Sensors* 4 (4 2014), pp. 281–290. ISSN: 22287477. DOI: 10.4103/2228-7477.144052.

- [30] Farhan Riaz et al. “Active Contours Based Segmentation and Lesion Periphery Analysis for Characterization of Skin Lesions in Dermoscopy Images”. In: *IEEE Journal of Biomedical and Health Informatics* 23 (2 2019). ISSN: 21682208. DOI: 10.1109/JBHI.2018.2832455.
- [31] Marco Ribeiro, Sameer Singh, and Carlos Guestrin. ““Why Should I Trust You?”: Explaining the Predictions of Any Classifier”. In: *ArXiv* (2016), pp. 97–101. DOI: 10.18653/v1/n16-3020.
- [32] Lavinia Ferrante di Ruffano et al. “Computer-assisted diagnosis techniques (dermoscopy and spectroscopy-based) for diagnosing skin cancer in adults”. In: *Cochrane Database of Systematic Reviews* (12 2018). ISSN: 1469493X. DOI: 10.1002/14651858.CD013186.
- [33] Wojciech Samek and Klaus Robert Müller. “Towards Explainable Artificial Intelligence”. In: *Lecture Notes in Computer Science (including subseries Lecture Notes in Artificial Intelligence and Lecture Notes in Bioinformatics)* 11700 LNCS (2019), pp. 5–22. ISSN: 16113349. DOI: 10.1007/978-3-030-28954-6_1.
- [34] Ramprasaath R. Selvaraju et al. “Grad-cam: Why did you say that? visual explanations from deep networks via gradient-based localization”. In: *Revista do Hospital das Clínicas* 17 (2016), pp. 331–336. ISSN: 00418781. URL: <http://arxiv.org/abs/1610.02391>.
- [35] Zhishun She, Y. Liu, and A. Damatoa. “Combination of features from skin pattern and ABCD analysis for lesion classification”. In: *Skin Research and Technology* 13 (1 2007), pp. 25–33. ISSN: 0909752X. DOI: 10.1111/j.1600-0846.2007.00181.x.
- [36] Wiebke Sondermann et al. “Prediction of melanoma evolution in melanocytic nevi via artificial intelligence: A call for prospective data”. In: *European Journal of Cancer* 119 (2019), pp. 30–34. ISSN: 18790852. DOI: 10.1016/j.ejca.2019.07.009.
- [37] S. M. Stricklin et al. “Cloudy and starry milia-like cysts: How well do they distinguish seborrheic keratoses from malignant melanomas?” In: *Journal of the European Academy of Dermatology and Venereology* 25 (10 2011), pp. 1222–1224. ISSN: 09269959. DOI: 10.1111/j.1468-3083.2010.03920.x.
- [38] Ki Hyun Tae et al. “Data Cleaning for Accurate, Fair, and Robust Models”. In: 2019. DOI: 10.1145/3329486.3329493.
- [39] Abdulrahman Takiddin et al. *Artificial intelligence for skin cancer detection: Scoping review*. 2021. DOI: 10.2196/22934.
- [40] Maen Takruri and Abubakar Abubakar. “Bayesian decision fusion for enhancing melanoma recognition accuracy”. In: *2017 International Conference on Electrical and Computing Technologies and Applications, ICECTA 2017* 2018-Janua (2017), pp. 1–4. DOI: 10.1109/ICECTA.2017.8252063.

- [41] Arthur Tenenhaus et al. “Detection of melanoma from dermoscopic images of naevi acquired under uncontrolled conditions”. In: *Skin Research and Technology* 16 (1 2010), pp. 85–97. ISSN: 0909752X. DOI: 10.1111/j.1600-0846.2009.00385.x.
- [42] B.H. Thiers. “Dermoscopy compared with naked eye examination for the diagnosis of primary melanoma: a meta-analysis of studies performed in a clinical setting”. In: *Yearbook of Dermatology and Dermatologic Surgery* 2009 (2009), pp. 378–379. ISSN: 00933619. DOI: 10.1016/s0093-3619(08)79154-8.
- [43] Erico Tjoa and Cuntai Guan Fellow. “A Survey on Explainable Artificial Intelligence (XAI): Towards Medical XAI”. In: *arXiv* (2019). ISSN: 23318422. DOI: 10.1109/tnnls.2020.3027314. URL: <http://arxiv.org/abs/1907.07374>.
- [44] Cancer Research UK. *Melanoma skin cancer statistics — Cancer Research UK*. 2019. URL: <https://www.cancerresearchuk.org/health-professional/cancer-statistics/statistics-by-cancer-type/melanoma-skin-cancer#heading-Three>.
- [45] Ezgi Unlu, Bengu N. Akay, and Cengizhan Erdem. “Comparison of dermoscopic diagnostic algorithms based on calculation: The ABCD rule of dermoscopy, the seven-point checklist, the three-point checklist and the CASH algorithm in dermoscopic evaluation of melanocytic lesions”. In: *Journal of Dermatology* 41 (7 2014), pp. 598–603. ISSN: 13468138. DOI: 10.1111/1346-8138.12491.
- [46] Zachary J. Wolner et al. *Enhancing Skin Cancer Diagnosis with Dermoscopy*. 2017. DOI: 10.1016/j.det.2017.06.003.
- [47] Yading Yuan and Yeh Chi Lo. “Improving Dermoscopic Image Segmentation With Enhanced Convolutional-Deconvolutional Networks”. In: *IEEE Journal of Biomedical and Health Informatics* 23 (2 2019), pp. 519–526. ISSN: 21682194. DOI: 10.1109/JBHI.2017.2787487. URL: <http://arxiv.org/abs/1703.05165><http://dx.doi.org/10.1109/JBHI.2017.2787487>.
- [48] Ihab S. Zaqout. “Diagnosis of Skin Lesions Based on Dermoscopic Images Using Image Processing Techniques”. In: *International Journal of Signal Processing, Image Processing and Pattern Recognition* 9 (9 2016), pp. 189–204. ISSN: 20054254. DOI: 10.14257/ijsp.2016.9.9.18.
- [49] Yongfeng Zhang and Xu Chen. “Explainable Recommendation: A Survey and New Perspectives”. In: (2018). URL: <http://arxiv.org/abs/1804.11192>.

()

Chapter 10

Tables

Chapter 11

Appendix